Submitted to Physical Review

UCRL-18996
Preprint

c.2

FRAGMENT PRODUCTION IN THE INTERACTION OF 5.5-GeV PROTONS WITH URANIUM

A. M. Poskanzer, Gilbert W. Butler, and Earl K. Hyde

July 1970

AEC Contract No. W-7405-eng-48

RECEIVED
LAWRENCE
RADIATION LABORATORY
SEP 30 1970
LIBRARY AND
DOCUMENTS SECTION

TWO-WEEK LOAN COPY

This is a Library Circulating Copy which may be borrowed for two weeks. For a personal retention copy, call Tech. Info. Division, Ext. 5545

LAWRENCE RADIATION LABORATORY
UNIVERSITY of CALIFORNIA BERKELEY

UCRL-18996 c.2

DISCLAIMER

This document was prepared as an account of work sponsored by the United States Government. While this document is believed to contain correct information, neither the United States Government nor any agency thereof, nor the Regents of the University of California, nor any of their employees, makes any warranty, express or implied, or assumes any legal responsibility for the accuracy, completeness, or usefulness of any information, apparatus, product, or process disclosed, or represents that its use would not infringe privately owned rights. Reference herein to any specific commercial product, process, or service by its trade name, trademark, manufacturer, or otherwise, does not necessarily constitute or imply its endorsement, recommendation, or favoring by the United States Government or any agency thereof, or the Regents of the University of California. The views and opinions of authors expressed herein do not necessarily state or reflect those of the United States Government or any agency thereof or the Regents of the University of California.

FRAGMENT PRODUCTION IN THE INTERACTION OF 5.5-GeV PROTONS WITH URANIUM*

A. M. Poskanzer, Gilbert W. Butler†, and Earl K. Hyde

Lawrence Radiation Laboratory
University of California
Berkeley, California 94720

July 1970

ABSTRACT

The energy spectra of nuclear fragments produced by the interaction of 5.5-GeV protons with uranium have been determined at several laboratory angles by means of dE/dx - E measurements with semiconductor detector telescopes. Individual isotopes of the elements from hydrogen to carbon were resolved and from nitrogen to argon the study was continued for the elements without isotopic separation. The evaporation-like energy spectra were integrated to obtain angular distributions and total cross sections for the isotopes of helium through carbon. Total cross sections for many rare isotopes were also estimated. The yield surface constructed from these cross sections has a ridge-like shape positioned one neutron in excess of the line of beta stability. The yields fall off more steeply on the neutron-deficient side and exhibit odd-even effects reflecting those of the mass surface. The energy spectra of the neutron-deficient isotopes differ from the others in that the high-energy parts of the spectra are more pronounced and flatter, and the angular distributions are more forward peaked.

Some of the energy spectra were fitted with calculated curves based on the isotropic evaporation of fragments from a system moving along the beam axis. The apparent Coulomb barriers obtained from this analysis were about one half

the nominal Coulomb barriers and the apparent nuclear temperatures fell in the 10 to 13 MeV range. For the highest energy fragments observed at 90° the apparent temperatures rose to 20 MeV. From the forward-backward shifts in energy it was deduced that the average velocity of the moving system is about 0.006 c and that there is a positive correlation between this velocity and the velocity of the fragments in the moving system. However, all of the data are more peaked forward in intensity than can be explained by this simple two-step model.

Radiochemical cross sections are also presented for the production of ^{7}Be from uranium, silver, and aluminum, and for ^{22}Na from aluminum.

I. INTRODUCTION

This paper describes an experimental study of fragments ejected from uranium targets bombarded with 5.5-GeV protons. Fragments emerging from a thin uranium target located in the external beam line of the Berkeley Bevatron were observed with a telescope of silicon semiconductor detectors. By simultaneous measurement of the partial energy loss in a thin transmission detector and of the total kinetic energy it was possible to distinguish the mass and atomic number of each fragment. Formation cross sections and energy spectra were recorded at five angles to the beam for the individual isotopes of hydrogen, helium, lithium, beryllium, boron, and carbon. Beyond carbon isotopic resolution was lost but it was still possible to distinguish individual elements up through argon (Z = 18) and the high-energy portions of the energy spectra were measured at three angles to the beam.

The substantial formation cross sections, the broad energy spectra, and the wide variety of the products which were observed reflect the complexity of these high-energy interactions. Every known particle-stable isotope of the light elements is formed with appreciable yield in the high-energy breakup of uranium. We took advantage of this fact during the early stages of this research to search for isotopes which were previously unknown and succeeded in making the first identification of ^{11}Li, ^{14}B, ^{15}B, and ^{17}C, as reported in two earlier publications.[1,2] Other new isotopes in this region have been reported by the use of a similar technique by a group at the Princeton-Pennsylvania accelerator,[3,4] and by the use of different techniques, by groups from Dubna[5-7] and Orsay.[8,9]

The characteristics of the light fragments cannot be discussed or interpreted without some consideration of the heavier mass products. The general yield pattern for these is known mainly from radiochemical measurements on many dozens of nuclides produced by the interaction of uranium with protons in the 1 to 30 GeV range. Other products have been determined by mass spectrometry, counting of volatile products in gas counters, neutron counting of delayed-neutron emitters, measurement of tracks in nuclear emulsions, etc. Although these measurements have been extensive they are still quite incomplete because of the massive task posed by the formation of hundreds of nuclear species. Most of the work has been done in the mid-mass region as reviewed by Friedlander.[10] Fission products constitute a major part of this group but the yield distribution is quite unlike that observed for uranium fission for bombardment energies of 50 to 500 MeV. Measurements of other characteristics of those products suggest that some mechanism other than normal fission contributes significantly. Above mass 170 there is a gradual rise in cross section which can be attributed to the spallation products.[11]

The conventional description of the mechanism of high-energy reactions divides the process into two stages.[12] In the first stage the incoming particle interacts with the individual nucleons in a quasi-free manner and develops a fast nucleonic cascade during which many nucleons or possibly even small nuclear aggregates are ejected. By the end of this first stage a group of interacting target nuclei is converted to a distribution of excited nuclei differing in Z, A, and excitation energy. In the second stage of the reaction the nuclear excitation is dissipated by the evaporation of nucleons or nuclear clusters, or by fission. Because the excitation energy is quite high many nucleons or clusters must be emitted before de-excitation is achieved. An assumption of this cascade-evaporation

mechanism is that the two stages are so well separated that the momentum of the final nucleus can be decomposed into momentum vector components from each stage. Critical tests of the applicability of this conventional two-stage model to the interaction of GeV protons with heavy nuclei have focused on the study of these momentum components.[13]

It has been suggested by some authors that the conventional model must be supplemented by other reaction mechanisms for GeV bombardment energies.[14,15] One such mechanism was formulated by Wolfgang et al.[14] under the name "fragmentation" to explain results obtained in the interaction of GeV protons with lead targets, particularly the behavior of such products as ^{18}F and ^{24}Na. Fragmentation is envisioned as a fast breakup of the nucleus into two massive partners induced by the breaking of many nucleon-nucleon bonds in a local volume of the nucleus. The complex cascades required for fragmentation might include as an essential element the formation and reabsorption of mesons.

Literature reports are contradictory on the necessity to invoke a fragmentation mechanism to explain observed fragment characteristics. Crespo, Alexander, and Hyde[16] measured yield and energy characteristics of ^{24}Na and ^{28}Mg produced in GeV proton bombardments of uranium and by an indirect analysis they concluded that the two-stage model could not adequately account for the data. Cumming, Cross, Hudis, and Poskanzer[17] investigated ^{24}Na production from bismuth bombarded with 2-GeV protons. By measurement of energy spectra at 3 angles to the beam and cross section as a function of angle they were able to make a direct test of the model uncomplicated by assumptions applied during the analysis. They were unable to obtain a self-consistent set of parameters to explain the angular and energy distributions on the basis of the two-stage model.

On the other hand, several attempts[18-20] to account for light fragments as evaporated particles in the de-excitation stage have been moderately successful. Particularly significant is the calculation by Dostrovsky, Davis, Poskanzer, and Reeder[21] of the formation cross sections for ^{9}Li, ^{16}C, ^{17}N, and other fragments as a function of bombarding energy for many targets including uranium. These computations involved extensive Monte Carlo calculations of the evaporation stage starting with a distribution of excited nuclei taken from previous Monte Carlo calculations of the cascade stage. The computed yields for these evaporated products reproduced the experimental trend of cross section with target mass quite satisfactorily.

Studies of energy spectra and angular distributions have been made by Crespo, Cumming, and Poskanzer[22] for ^{91}Sr, ^{99}Mo, ^{103}Pd, ^{131}Ba, and ^{140}Ba from uranium and by Crespo, Cumming, and Alexander[23] for ^{149}Tb from gold. Both sets of authors concluded that the observed spectra and angular distributions of all these isotopes were consistent with a two-step model.

Katcoff, Baker, and Porile[24] measured ^{8}Li fragments by emulsion techniques from Cu, Ag, and Au targets bombarded with 2-GeV protons and compared the observed energy spectra with spectra computed from the cascade-evaporation model. Distributions of residual nuclei obtained from a previous Monte Carlo calculation of the cascade step were subjected to a second Monte Carlo calculation to determine the properties of ^{8}Li fragments formed by evaporation from these excited residual nuclei. The authors concluded that evaporation theory can account for some of the features of ^{8}Li emission in high-energy interactions. The main shortcomings of their calculation lie in its failure to match the strong forward peaking of the angular distribution and in its inability to

account for the emission of the highest energy fragments. Grigor'ev et al.[25] used nuclear emulsions to study the characteristics of ^{8}Li emitted by thorium targets bombarded with 660-MeV protons. They also employed a cascade-evaporation Monte Carlo technique to compute the expected energy spectrum for comparison with the data. These authors found very poor agreement of theory and experiment and concluded that the observed fragments could not be described by statistical evaporation theory.

In spite of the considerable amount of work that has been done a completely definitive test of the adequacy or inadequacy of the cascade-evaporation model has not been made because of the sparseness of the experimental data and the great complexity of the Monte Carlo calculations for the two reaction stages, which forces the use of many approximations. These difficulties are compounded by major uncertainties in important details of the theory. However, interesting new ideas concerning evaporation from nuclei before equilibration of energy, so called pre-equilibrium emission,[26-29] suggest promising ways for future treatment of the indeterminate region between the two stages of the cascade-evaporation model.

The experimental results presented in this paper cannot by themselves resolve the questions raised above. It is clear, however, from an examination of the published literature, that the determination of yields and energy spectra at several angles to the beam for a variety of products is a prerequisite for a stringent test of the calculated results of any reaction mechanism. It is a major purpose of this work to provide an extensive set of such data for a large number of fragments for a specific reaction system.

The semiconductor detector telescope seemed the appropriate tool to choose for this purpose. Past developments in particle identification systems

at this laboratory[30] provided the capability for clean identification of particles by nuclear charge and mass and this capability is ideally suited to the study of the wide variety of fragments from high-energy reactions. The method does suffer from a low-energy cutoff that increases with fragment charge but the majority of the fragments with $Z \leqslant 6$ in the case of uranium targets have energies exceeding this cutoff energy. The semiconductor detector telescope then makes it possible to measure all fragments above this cutoff energy which have lifetimes longer than the time-of-flight to the detectors. Since this time is of the order of ten nanoseconds the only fragments which decay before detection are those formed in excited states unstable toward particle emission. Products like ^{8}Be or ^{9}B which are particle-unstable even in the ground state are missing entirely from the particle spectra. This same remark applies, unfortunately, to the hyperfragments which are known to be formed in appreciable yield in the interaction of 5-GeV protons with complex targets;[31] the longest decay time for a hyperfragment is of the order of 10^{-10} seconds.

The advantages of the semiconductor detector telescope are that in a single in-beam experiment it is possible to identify all the isotopes of several elements, including stable and radioactive forms. In addition, the energy spectrum of each of the identified nuclides is obtained. In a series of measurements taken at several angles to the beam the change in the energy spectra as a function of angle can be studied and by integration of these energy spectra it is possible to determine the angular distributions of the products. This experimental method is thus much more powerful than the radiochemical or emulsion techniques used in previous studies of fragments from uranium. In fact, radiochemical yields have been measured for only those few nuclides which have suitable half lives, and it has been emphasized that in this light mass region

it is the stable isotopes which have the highest yields.[15] A summary of all the previous data on yields of products below mass 30 from uranium bombarded with GeV protons is shown in Table I.[32-37] Previous studies of energy spectra of fragments from any heavy element bombarded with GeV protons have been even more limited. One is the study of ^{24}Na produced in the bombardment of bismuth with 2-GeV protons cited earlier.[17] Others are emulsion studies done by Katcoff on ^{8}Li fragments from uranium[38] and gold[24] bombarded with 3-GeV protons, by Gajewski, Gorichev, and Perfilov[39] on ^{8}Li fragments ejected by lead nuclei bombarded with 9-GeV protons, and by Gorichev, Lozhkin, and Perfilov[40] on Li, Be, B, and C fragments from tantalum and lead bombarded by 2 to 9-GeV protons.

Semiconductor detector telescopes[41,42] and other particle identification techniques have been used previously[43,44] for measurement of Li, Be, B, and other light fragments emitted as a third particle in spontaneous fission or thermal-neutron induced fission. The reported fragment characteristics are quite different from those observed in our high-energy study.

II. EXPERIMENTAL

A. General

The experiments were done in a 36-in. diameter evacuated target chamber installed in the 5.5-GeV external proton beam of the Bevatron. The beam consisted of 0.8 sec pulses containing about 3×10^{11} protons, repeated every six seconds. This beam was focused by several sets of quadrupole magnets and its size at our target location, five feet upstream from a focal point, was typically 1/2 in. wide by 5/8 in. high. However, there was a diffuse halo of lesser intensity over a considerably larger area even though there were no other targets upstream from ours. The contribution of this halo to background effects was reduced by the use of large beam entrance and exit pipes and the use of a target support with a minimal amount of material within several inches of the central beam spot. A drive mechanism located in the top of the chamber could be remotely operated to lower the target into the beam or to withdraw it. The target was rotated so that the perpendicular to the target was at either 55° or 125° to the beam depending on whether the fragment telescope was in the forward or backward hemisphere.

The fragment telescope consisted of three or four phosphorus-diffused or lithium-drifted silicon detectors with associated collimators mounted on an aluminum block which in turn was mounted on a movable arm which had its pivot point in the center of the chamber directly under the target. The position of the aluminum block supporting the detectors could be adjusted radially before the chamber was closed. The angular position of the movable arm could be adjusted remotely. Possible angular settings of the telescope with respect to the beam line ranged from 20° to 160°.

The fragment telescope consisted of one or two ΔE (transmission) detectors of 20 to 250 μm thickness, an E detector of 100 to 5000 μm thickness, and a rejection detector, E_{rej}, which was used in an anticoincidence mode to exclude long range particles which did not stop in the E detector. These detectors were incorporated in an identifier system of the power-law type.[30] The overall system is shown in Fig. 1 and a detailed description may be found elsewhere.[30,45-47] Particle identification was based on the fact that the range, R, of any particle of interest in this study could be approximately expressed by the empirical relationship, $R = a\mathcal{E}^b$, where $\mathcal{E}$ is its energy, a is a proportionality constant with a specific value for each particle for a given value of b, and b is an exponent which, in the energy range of interest here, varies with Z approximately as follows: b = 1.7 for Z = 1 and 2, b = 1.6 for Z = 3 and 4, b = 1.4 for Z = 6-11, and b = 1.2 for Z = 12-18. If we define T as the thickness of the ΔE detector it is possible to derive from the above relationship the following expression,

$$T/a = (E + \Delta E)^b - E^b \quad ,$$

which has the useful feature that the quantity T/a is a constant for a particle with a given Z and A regardless of the energy of the particle. The particle-identifier system uses analog circuitry to perform the operations on the E and ΔE signals given on the right side of this expression and to generate an output signal proportional to T/a for each recorded particle. This signal is referred to as the particle identification signal. At the same time the total energy (E + ΔE) also appears as an output signal.

In some experiments in which the best resolution of neighboring isotopes was required the telescope included two ΔE detectors and the signals

were manipulated in a way to derive two different identification signals. The identification was accepted only if these two signals agreed within preselected limits. In this case the final output signal was obtained by summing the signals from the two ΔE detectors. (See Ref. 45 for a discussion of double ΔE systems of this type.)

In the operation of the particle-identifier system the value of the exponent b was determined empirically by collecting particle spectra for short periods of time at different settings of the circuit element which controlled b until the best particle spectrum was obtained. Decisions on the most likely range of choices of b and other matters concerning setup for the experiments were greatly facilitated by the use of range-energy and energy-loss computer programs written at this laboratory.[48,49]

The particle-identifier signal and the total energy signal for each event were passed to an analog-to-digital converter and from there to a small computer. After a preliminary collection of data, digital markers were set on the oscilloscope display around specific peaks in the particle spectrum. These were used in subsequent data collection to sort event-by-event and to construct histograms of the energy spectra corresponding to specific nuclides in the particle spectrum.

Accurate beam monitoring was of great importance. A beam monitoring device which measured the current of secondary electrons knocked out of aluminum foils in a vacuum chamber was installed in the beam line downstream from our chamber and provided us an approximate measure of the beam intensity useful for set-up purposes but quite inadequate for quantitative work. For precise relative measurement of the beam intensity we installed a monitor telescope on an

aluminum block fixed at 90° to the beam and located on the opposite side of the beam line from the fragment telescope. This monitor telescope, which was always positioned at the same distance from the target as the fragment telescope, consisted of a 136-mg/cm^2 aluminum absorber followed by 121-μm and 117-μm phosphorus-diffused silicon transmission detectors. This telescope, with appropriate amplitude and coincidence requirements set on its electronic pulses, recorded a spectrum consisting of 90% alpha particles (the remainder being ^{3}He and ^{6}He particles) with an energy range of 40.0 to 42.8 MeV (incident on the aluminum absorber). High-energy alpha particles were used to monitor the experiments because their yield was not distorted by contributions from the interaction of stray protons with the low-Z materials of construction in the chamber or target mount and also because negligible corrections to the monitor were required when targets of different thicknesses were used. In order to convert these relative yields based on the monitor telescope to an absolute basis it was necessary to know the yield of at least one product. For this purpose we determined the radiochemical yield of ^{7}Be, as discussed in the Appendix.

B. Details of Targets, Detectors, and Electronics

1. Uranium targets. Three different uranium targets 1.5 in. wide by 1 in. high were used during the course of these experiments. All of them were centered on a piece of 0.00025 in. Mylar (1 mg/cm^2), which was in turn fastened to an aluminum frame that had a 6 in. wide by 3.5 in. high hole in it. A 27.5 mg/cm^2 uranium metal target was used for the investigation of the high energy portions of the fragment energy spectra while a 10 mg/cm^2 uranium metal target (obtained from Oak Ridge National Laboratory) was used to study intermediate energy spectra. Low energy spectra were recorded on fragments from a target made by evaporating UF_4 to a thickness of 0.7 mg/cm^2 (0.53 mg/cm^2 of U) onto a Mylar backing. Background measurements were made to determine the contribution of the Mylar backing to the fragment energy spectra and the monitor counting rate. These contributions were usually small except in experiments made on the lighter isotopes with the UF_4 target.

2. Detectors and collimators. Most of the detectors were phosphorus-diffused silicon transmission detectors 5 mm wide by 7 mm high, except for the E_{rej} detector which was 8 mm wide by 10 mm high. These detectors were made by the semiconductor device group of the Nuclear Chemistry Division. Each detector was supported on an aluminum plate which was positioned above the aluminum block base by mounting pins which assured the accurate alignment of the detectors with respect to each other and at the same time the easy substitution of one detector for another. Rectangular copper collimators with dimensions of 4 mm wide by 6 mm high were placed in front of the first detector and in front of the E detector. Both collimators were 0.80 mm thick except in those experiments involving the study of Z = 1 and 2 fragments in which case both

collimators were 1.86 mm thick. The distance from the center of the target to the E detector collimator was 21.7 cm for low-yield experiments and 41.6 cm for high-yield experiments.

In experiments whose purpose was to measure the energy spectra of particles whose ranges were too great for the available phosphorus-diffused detectors (300 μm or less) circular lithium-drifted silicon detectors of 1 cm diameter were used. In order to reduce the leakage current and to decrease the rise time of the pulse from E detectors of this type with thickness ≥1.5 mm a thermoelectric cooler was used to chill the detectors to -20°C.

Table II is a listing of the many counter telescopes which were used in this work. The fundamental reason for the variety of telescopes was that it was not practical to measure the energy spectra over a wide range and to achieve good particle resolution for all particles with a single choice of thicknesses for the ΔE and E detectors. The quality of the particle spectra obtained with three different telescopes, all employing a 61-μm ΔE counter is shown in Fig. 2. The particle spectra for the telescopes using a 20-μm ΔE counter were not as good but they allowed us to extend the measurements to lower energies. Parts of the energy spectra always overlapped and in some cases where there was a discrepancy the 20-μm data were normalized to the data of the thicker telescope. Also in the case of telescopes using a 5-mm E counter, pile-up effects distorted the particle spectra and these results were normalized where they overlapped with data from thinner telescopes. In cases where two ΔE counters were used, the valleys between the peaks were deeper and then the rarer isotopes could be distinguished (see Ref. 1,2). Figure 3 shows a particle spectrum from a telescope with a 20-μm ΔE counter in which element resolution was achieved but individual isotopes were not separated.

3. Electronics. Each detector was connected by a short length of cable to the input of a charge-sensitive preamplifier, which in turn was connected by 100 ft of 125-Ω cable to the counting area. The signals were fed into linear amplifiers with delay-line shaping and an integrating time constant of 0.1 μsec. Amplifier clipping lines were 0.4 μsec long except for those experiments utilizing thick (≥ 3 mm) E detectors, in which case the clipping lines were 0.8 μsec long. A pile-up rejector, which had a resolving time of 50 nsec, was used to reduce the background due to chance coincidence events. The pile-up rejector (details are described in Ref. 45) generated two different logic signals; the first one was sent to the E_{rej} coincidence circuit whenever one of the leading-edge discriminators in the pile-up rejector detected an event in any one of the fragment detectors. The second logic signal, which was the valid event signal, went to the master coincidence circuit whenever an event met all the requirements of the pile-up rejector. A crossover pickoff signal from the E_{rej} detector was fed into the E_{rej} coincidence circuit and if there was a coincidence between this signal and the signal from the pile-up rejector, then an anticoincidence signal was sent to the master coincidence circuit. This E_{rej} coincidence requirement greatly reduced the dead time due to anticoincidences because most of the E_{rej} counting rate was not correlated with counts in the other detectors. The valid event signal from the pile-up rejector was not used as the input to the E_{rej} coincidence circuit because it occurred too late.

The determination of an energy scale up to 200 MeV was important for these experiments and it will be discussed in some detail because it differed from conventional pulser techniques. A pulser, which was located in the counting area, supplied both a dc reference voltage and a frequency signal to a transistor chopper, which was attached directly to the test input of the preamplifier.

(See Ref. 45 for more details of this pulser.) The maximum voltage step that was fed into the preamplifier test capacitor was 1.00 V, and this voltage, when fed into a carefully calibrated 4.425 pF test capacitor, corresponded to an energy of 100 MeV absorbed in a silicon detector. These numbers are based on the accurate determination by Pehl, Goulding, Landis, and Lenzlinger,[50] of the average energy expended for electron-hole pair generation in silicon, which was found to be 3.62 ± 0.02 eV at room temperature. This pulser was always found to be in agreement with low energy alpha particles whenever a natural alpha-source calibration was made.

C. Computer Systems and Programs

1. On-line PDP-8 system. The on-line computer system that was used to record the data is shown in Fig. 4. A Digital Equipment Corporation PDP-8 twelve-bit 4096-word computer (cycle time of 1.5 μsec) was interfaced, through a data break system, to a movable-head disk (Data Disc, Inc.) with 128 different tracks, each of which contained 29 individually accessible sectors of 128 twelve-bit words. The disk, which made one complete revolution every 50 msec, also had three fixed-head tracks, each containing 29 sectors of 128 words. Two of these fixed-head tracks were used, on an alternating basis, for the hardware oscilloscope display, (this freeing the computer from continuous display calculations) while the third fixed-head track was used as a buffer storage area. The large memory of the movable-head disk permitted the permanent storage of both compiled and uncompiled computer programs, thereby largely eliminating the need for paper tape input/output and greatly facilitating the editing and recompilation of programs. The computer was also interfaced through the data break

system to an Ampex TM7 IBM-compatible magnetic tape unit which was capable of writing and reading at 556 or 800 bytes per inch. The computer was interfaced to several scalers which recorded the various counting rates that were essential for the accurate determination of cross sections relative to the monitor.

It was mentioned in Sec. A that the output of the particle identifier system consisted of a particle identification pulse proportional to $(\Delta E + E)^b - E^b$ and an E_{total} pulse equal to $\Delta E + E$. These two pulses, together with the ΔE and E signals, were presented to the computer system for each event. Pulse stretchers, a multiplexer,[51] and an analog-to-digital converter of the successive binary-approximation type[52] was used to encode these four input pulses one at a time and send them to the computer as 10-bit numbers. The ADC took about 25 μsec to digitize each pulse and the multiplexer-ADC-computer system processed one four-parameter event in approximately 200 μsec.

Because of the pulsed mode of the beam, the following technique was used for data collection by the computer.[53] When the beam-on signal was received by the computer, a data-taking program was read into the computer from the movable-head disk in approximately 0.15 sec. This program used a buffer system (each buffer contained 127 events) to write the incoming data onto one of the fixed-head tracks of the disk, as well as to write the raw data onto magnetic tape. After the beam went off, the computer used the data on the fixed-head track to update the histograms, which were stored in double precision on the movable-head disk. Then the display programs were read into core from the disk and the oscilloscope displays were recalculated. The raw-data magnetic tape could be used to sort the data after the experiment if necessary. It also provided the flexibility of reprocessing the data digitally at the Control Data Corporation

6600 computer to do particle identification and data sorting entirely independent of the analog electronic system of particle identification used on-line. This feature of the data reduction system is not discussed further because all results presented in this paper were obtained from the analog system.

Three different kinds of histograms were calculated by the computer and any one of them could be displayed on command. The first histogram was a 512-channel particle spectrum. Digital markers could be set around any peak in the particle spectrum and viewed on the oscilloscope. The incoming data were sorted on the particle identification pulse, and for each pulse which fell between a pair of markers the corresponding total energy pulse was stored in an appropriate buffer. A total of 24 digital markers was available, thus allowing the simultaneous storage of 12 different energy spectra, each of which could be displayed as a 128-channel energy histogram. The third kind of histogram was a two-parameter matrix of particle spectrum versus total energy which could be shown as either a contour or an isometric display. These latter displays were quite useful in determining whether the proper value of the exponent b was being used in the particle identifier.

2. Final data reduction at CDC-6600. Whenever a particular experiment was completed, the updated histograms were written onto magnetic tape and these tapes were taken to the CDC-6600 computer for further processing by different Fortran computer programs written by one of us (G.W.B.). The first program transformed the raw energy spectra to histograms corrected for absorption in the target and in any absorber, such as the dead layers of the detectors (typically a total of 1.2 μm thick). The analytical method used for these range-energy corrections was obtained from Bichsel and Tschalaer,[54] and was based on an

exponential fit of the type $R = a\mathcal{E}^b$ to calculated range-energy tables. In general, several sets of parameters were needed to cover the energy range of each fragment that was studied. It should be pointed out, however, that these corrections to the energy spectra were usually small. After corrections were made for the fraction of the events rejected by the pile-up rejector, and the fraction of the events lost because of computer dead time, the corrected counts per MeV relative to the monitor were calculated. When two ΔE detectors were used the data were also corrected for the fraction of the events that were not accepted because of the requirement that the two identifications agree. Linear or semi-logarithmic plots of these corrected energy spectra were obtained from this program, which also produced semi-logarithmic plots of the particle spectra.

The second computer program, which displayed the corrected energy spectra on a large oscilloscope, was an on-line CDC-6600 program that worked on an interrupt basis. A light pen and a command console were used to communicate with the computer. It has been mentioned previously that it was necessary to take data in two or more experiments with different telescopes in order to cover the major regions of the energy spectrum. This program was capable of making background subtractions and plotting the data for each nuclide from the several different experiments on one oscilloscope display. A light pen was used to draw a smooth curve through the combined data points and in most cases it was possible to extrapolate this curve to zero energy. Examples of semilogarithmic oscilloscope displays of three sets of data points and of the smooth curves drawn through the data are given in Fig. 5 for three different nuclides. The smooth curves were integrated by the computer to determine the relative differential cross sections ($d\sigma/d\Omega$). These angular distributions were then integrated to

obtain total cross sections. All of these relative cross sections were normalized to absolute cross sections on the basis of the radiochemical determination of the yield of ^{7}Be produced from the bombardment of uranium with 5.5-GeV protons. This cross section was determined to be 17.6 mb and is described in the Appendix. Many of the figures presented in this paper were drawn on the basis of a preliminary value of 16.0 mb; in these cases the figure captions indicate that the data should be raised by the factor 1.10.

III. RESULTS

The results for the laboratory energy spectra are shown in Figs. 6 to 12. In general the curves have the appearance of Maxwellian evaporation spectra and the data in most cases cover an adequate range below and above the maximum yield to reveal the major characteristics of the distribution and to permit the integration of the curves in order to derive the angular distributions. For the hydrogen isotopes and for ^{3}He the particle ranges were so great that it was not possible to measure the high-energy regions of the spectra with the semiconductor detectors used in these experiments. Inspection of the series of figures reveals that the experimental low-energy cutoff moves to higher energies as fragment Z increases until at carbon it falls near the maximum in the energy spectrum. Nitrogen isotopes could not be resolved using our thinnest ΔE detector and therefore near the maximum the energy spectrum could not be measured. Thus we were unable to perform the integrations required to determine the angular distributions and total cross sections for individual nitrogen isotopes.

For the isotopes of the elements helium through carbon a feature of the curves is that the cross sections in the laboratory system increase at the more forward angles and the maxima move to slightly higher energies, as would be expected if the evaporating nucleus has an appreciable forward momentum component. It may also be remarked that a greater fraction of the energy spectrum of neutron-deficient isotopes like ^{3}He and ^{7}Be occurs at high energy than is the case for the other isotopes of these elements. This is much more evident in Fig. 13 where all the curves at 90° are displayed in a semilogarithmic plot. Here all the solid curves display about the same slopes at high energy, but the broken curves, which represent the most neutron-deficient isotope of each element,

are distinctly flatter. Within the framework of the cascade-evaporation model, this would indicate a higher temperature or larger deposition energy for those cascades which lead to neutron-deficient products. Also in this figure it can be seen how the peaks in the curves move to higher energies as Z increases, as would be expected from the increased Coulomb barrier.

In Fig. 14 the element energy spectra are displayed for the three angles that were measured. It is surprising that the differential cross sections for carbon through argon are so nearly equal over the observed energy range. Of course the higher Z elements would peak at higher energy, and therefore the total cross sections probably decrease somewhat with increasing Z. In the backward direction the differential cross sections even increase with Z, indicating that the angular distributions are becoming more isotropic as the products get heavier.

The laboratory angular distributions that were obtained by integrating the energy spectra of those isotopes that could be extrapolated to zero energy are shown in Fig. 15. Except for the hydrogen isotopes, which have a significant cutoff on the high energy side, all the angular distributions are similar. However, closer inspection shows that some of the neutron-deficient isotopes, for example ^{7}Be and ^{11}C, are more peaked forward. If the ^{3}He data were not cut off at 100 MeV its angular distribution also would be more peaked forward, as can be seen from Fig. 7. The angular distributions were also integrated to obtain the fractions forward and the fractions backward for all the isotopes and the results are presented in Table III.

Integration of the angular distributions yields the total production cross sections shown in Fig. 16. In the case of ^{3}He an extrapolation of the

energy spectra to higher energies was made which resulted in the number shown being 27% larger than that obtained from the data below 100 MeV. In the case of the hydrogen isotopes an extrapolation to higher energies was not feasible and therefore no cross sections are shown. All the other approximate cross sections were obtained from ratios of peak areas in our best particle spectra. For this purpose our published spectra,[1,2] as well as a few unpublished spectra were employed. The procedure used was to make a semilogarithmic plot of the ratio of a known cross section to its peak area versus the channel number of the peak. Then smooth curves of the experimental bias were drawn for each Z and these were simply extrapolated for the rarer isotopes. Ratios of cross section to peak area were read off these curves and used with rare isotope peak areas to obtain the numbers shown. In addition to the obvious problem resulting from an extrapolation, this procedure emphasized the high energies and forward angles because the telescopes used had thick ΔE counters and were oriented at 30° to 45° to the beam. This should not cause much trouble for neutron-excess isotopes, but it probably means the cross sections given for ^{8}B and ^{10}C are too high. The contour lines have been drawn in Fig. 16 by logarithmic interpolation. For the purpose of extending these contour lines through nitrogen, rough estimates were made of the cross sections for the nitrogen isotopes.[55]

The main feature of the ridge-like yield surface is that it is fairly smooth with small wiggles along the sides. This smoothness is surprising because many of the isotopes have only one bound level. The wiggles along the sides are the result of an odd-even effect. This can be seen from the fact that in most of the even-even nuclides the contours tend to bulge out and in the odd-odd nuclides they tend to dip in. In evaporation calculations it is known that

there are two causes of odd-even effects which go in opposite directions. The odd-even effects in the mass surface, which enter through the Q-values, favor the yields of even-even nuclei and disfavor odd-odd nuclei. The odd-even effects of the level density, which enter through the parameter δ, do the reverse. It is clear that the odd-even effects of the mass surface are reflected in the present data. In the yield surface the ridge lies on the neutron-excess side of the valley of beta stability, as can be expected because uranium has many more neutrons than protons. The ridge is about one neutron in excess of the line of beta stability. The yields fall off more steeply on the neutron-deficient side, perhaps even more steeply than indicated in Fig. 16 because our estimate of the ^{8}B and ^{10}C yields may be too high. As an example of this steep drop off we cite the fact that we did not observe ^{9}C. The characteristics of the neutron-deficient isotopes--namely, low yields, more pronounced forward peaking, and more pronounced and flatter energy spectra at high energy--are all consistent with their formation as a result of higher-deposition-energy events in the knock-on cascade.

The cross sections were summed at each A and also at each Z to give the mass-yield and charge-yield data shown in Table IV. In order to extend the charge-yield data up to sodium the element energy spectra of Fig. 14 were integrated with the help of the curve fitting program to be described below. The cross sections are plotted in Fig. 17. Of course there are no particle-bound nuclei at mass 5 and the dip at masses 8 and 9 are due partly to the absence of ^{8}Be and ^{9}B. If one corrects both curves for the missing particle-unstable nuclides as estimated from the contours of Fig. 16, then the dips fill in somewhat. In the mass yield curve, except for mass 9, the odd A isotopes are higher

and, in the charge yield curve, even though the effect is much smaller, the even Z nuclei tend to be slightly higher. Since for each even A there should be as many odd-odd nuclei as even-even, one would expect the odd-even effect to disappear in the mass yield curve. The residual effect seen is probably due to the narrowness of the yield surface and the position of the ridge with respect to these particular isotopes. The charge yield curve has decreased to a level of 31 mb at Z = 11. This would indicate that the mass yield curve should continue to decrease to about the 15-mb level at an A of about 24. The integral of the charge yield curve from lithium through sodium is 850 mb.

The estimation of experimental errors on all the results presented here is quite difficult. Some of the better energy spectra were shown in Fig. 5. Repeated integrations of these curves with different extrapolations to zero energy always gave agreement to better than 5% for the areas under the curves. However, of the angular distributions shown in Fig. 15, those for ^{8}He, ^{9}Li, and the carbon isotopes are less accurate. The cross sections shown in Fig. 16 are probably accurate to 10% for those obtained by integration of their angular distributions and to 30% for those estimated for the rare isotopes from particle spectra at only one angle. In addition the ^{8}B and ^{10}C cross sections may be systematically high. Of course to all these errors must be added the 9% absolute error of the ^{7}Be cross section which is described in the Appendix.

IV. DISCUSSION

A. General

Although the data presented in this work are useful for learning the characteristics of fragment production, the ultimate purpose of these measurements, as mentioned in the introduction, is to obtain a better understanding of the interaction of high energy protons with complex nuclei and also the de-excitation of highly excited nuclei. As a preliminary form of analysis we have done qualitative curve fitting to some of our spectra employing a reasonable functional form having a small number of parameters. The purposes of this curve fitting were threefold. First, we thought it desirable to test the data for consistency with the two-step model. This is a necessary requirement for later interpretation of the data in terms of the cascade-evaporation model as it has been applied in the past. Second, because of the mass of graphical data in this paper, it was thought that a few parameters describing the data and the trends in the data would be useful. However, it was realized that quantitative fits to all of the spectra with a simple functional form would not be possible. Third, we wanted to integrate some of the element energy spectra to extend the charge yield curve beyond carbon. It was thought that fitting a simple functional form and extrapolating the parameters of this fit to the incomplete higher Z curves would be the best method.

The functional form chosen was that of a smeared Maxwellian shifted by an effective Coulomb barrier and isotropically distributed in a system moving forward with respect to the laboratory system. Thus in the moving system the energy spectrum of a fragment was taken to be

$$P(\varepsilon) = \sum_{k=\langle k \rangle - \Delta}^{\langle k \rangle + \Delta} (\varepsilon - kB)\, e^{-(\varepsilon - kB)/\tau}, \qquad \varepsilon > kB \quad ,$$

where τ can be called the nuclear temperature and $\langle k \rangle B$ the effective Coulomb barrier. The smearing, needed to reproduce the widths of the experimental spectra, was achieved by summing calculations for several values of k from Δ below $\langle k \rangle$ to Δ above $\langle k \rangle$. The nominal Coulomb barrier, B, was calculated with a radius parameter of 1.44 F and with the assumption that the emitting nucleus was $^{220}_{86}Rn$. The energies were corrected for recoil and related to a velocity in the moving system, V, by the equation

$$\frac{220-A}{220}\,\varepsilon = \frac{1}{2}\, m\, V^2 \quad .$$

The law of cosines was neglected and for the 90° spectra, the velocity in the lab, V_L, was taken equal to V. Thus at 90° the laboratory energy, E, was equal to $\varepsilon(220-A)/220$. To calculate V_L for the 20° and 160° spectra the velocity of the moving system, v, was simply added to and subtracted from V, respectively. The laboratory cross section was calculated from

$$\frac{d^2\sigma}{dE\,d\Omega} = P(\varepsilon)\,\frac{E}{\varepsilon}\,\frac{d\varepsilon}{dE} \quad .$$

This is proportional to $P(\varepsilon)\sqrt{E/\varepsilon}\,/(dV_L/dV)$. The quantity dV_L/dV was not equal to unity because it was found necessary to introduce a correlation between v and V. The correlation function adopted was[23]

$$\frac{v - \langle v \rangle}{\langle v \rangle} = n\,\frac{V - \langle V \rangle}{\langle V \rangle} \quad .$$

The quantity $\langle V \rangle$ was taken to be the root-mean-square V obtained from the average energy, $\langle \varepsilon \rangle$, which is equal to $\langle k \rangle B + 2\tau$ for Maxwellian spectra. Thus the parameters used in this fitting procedure were τ, $\langle k \rangle$, Δ, $\langle v \rangle$, and n. The fitting was done simply by comparing families of computer-calculated curves to the data and selecting by eye the best fits. An example is shown in Fig. 18. The parameters τ, $\langle k \rangle$, and Δ were adjusted for the 90° data, $\langle v \rangle$ from the shift of the peak between the 20° and 160° data, and n from the change in slope above the peak between the 20° and 160° data. A more sophisticated fitting procedure was not justifiable, because even with these five parameters good fits were not obtained. The major discrepancy was that the data indicated that more than one value of τ was necessary. However, instead of complicating the functional form by adding more parameters we fit the data mainly near the peaks of the curves, and in addition we obtained the apparent τ at the highest energies measured.

The resulting parameters are shown in Table V for some representative isotopes and for the elements through Na. The second column lists B, the nominal Coulomb barrier calculated by the simple prescription described above. The third column lists $\langle k \rangle$, the fraction of this nominal barrier which appears to fit the data. For the last few elements this parameter is less well determined and obtained partly by extrapolation from the lighter elements. For the lightest elements the effect of tunnelling through the Coulomb barrier is included in this constant. However, the striking feature is the constancy of the effective Coulomb barrier at about one half the value of the nominal Coulomb barrier. This conclusion is only slightly affected by uncertainties in the choice of the radius parameter or in the choice of the evaporating nucleus. The fourth column, Δ, is not the uncertainty in $\langle k \rangle$, but the

amount of smearing of k needed to fit the widths of the spectra on the low energy sides of the peaks. This is the least well determined of all the parameters since it is sensitive to the data points just above the low energy cutoff. The fifth column lists the experimentally observed energies of the peaks in the 90° spectra.[56] The sixth column lists τ, the apparent temperature obtained from energies just above the peak. The values are all 10-13 MeV except those for ^{4}He which is lower (6 MeV) and ^{7}Be which is higher (15 MeV). The seventh column lists τ_{HE} the apparent temperature obtained from the slopes of the 90° spectra at the highest energies measured. It is seen that the spectra of the heavier elements tend to exhibit a single temperature up to the highest energies measured, while the lighter isotopes, especially the neutron-deficient ones, exhibit very high apparent temperatures in the high energy portion of their spectra. How prominent these high energy regions are is not contained in Table V but can be seen in Fig. 13. For most of the isotopes they represent a tiny fraction of the total yield. However, for all the neutron-deficient isotopes they are more significant. The last column contains $\langle v \rangle /c$, the average velocity of the moving system in units of the velocity of light. This was taken from the shifts of the peaks between the 20° and 160° spectra and should actually be divided by the cosine of 20° (0.94). Except for ^{4}He it appears to average about 0.006 which is 0.18 $\sqrt{\text{MeV/amu}}$.

In the absence of a correlation between V and v the slopes at high energy would be equal at all angles. It is obvious in Figs. 14 and 18 that the high energy data are flatter at the forward angles and steeper at the backward angles. This was accounted for by a positive correlation with a value for n, the correlation parameter, equal to 2 in all cases. A positive correlation is consistent with the higher energy evaporated fragments coming from the higher

deposition energy knock-on cascades which are known to have higher deposition momenta. This value of n was well determined for the element energy spectra but not so well determined for those isotopes which prominently exhibited multiple values of τ. However, there is no doubt that in all cases the value of n was positive and significant. Such a positive value causes the peak heights at the forward angles to be lower than at the backward angles. This is clearly at variance with all the data shown in Figs. 7-11. The case for ^{11}B is shown in Fig. 18. The calculated curves cannot account for the amount of forward peaking exhibited by the data. This is also true for all the other data in this paper. If n were set equal to zero, the conclusion would not be changed because the value of n does not change the area of the curves. The discrepancy in peak heights would not be as great, but then the regions just above the peaks would disagree more and in fact exhibit the wrong slopes. The problem may be stated simply as follows. When one goes from backward to forward angles, the value of $\langle v \rangle$ inferred from the increase in energy of the peaks is not sufficient to explain the increase in heights of the peaks. Thus we must conclude that the angular distributions are peaked forward in this moving system or, consequently, that the two-step model is not valid for these data.

Thus high nuclear temperatures and forward-peaked angular distributions are characteristics of these reactions. It may be that eventually both these effects will be calculable with a model for pre-equilibrium evaporation which smoothly describes the transition from the knock-on cascade to the conventional evaporation. Alternatively, some other feature of high-energy reactions may be the cause of these effects.

Another dramatic characteristic is that the fitted Coulomb barriers are only about one half the nominal Coulomb barriers. In order to investigate the effect of the distortions[57] of the fragment and the heavy residue in lowering the Coulomb barrier we have looked at the process as very asymmetric liquid-drop fission. First, instead of considering tangent spheres with a radius parameter of 1.44 F, as was done to calculate the nominal Coulomb barrier values shown in Table V, we chose to calculate the separation of the two fragments by using a radius parameter of 1.22 F and adding an extra 1.7 F to account approximately for a neck between the fragments. For spheres this happens to reproduce almost exactly the nominal barrier values of Table V. However, now we allow the spheres to distort to collinear prolate spheroids. Tables for the potential energy surface of such a system have been calculated.[58] For example, for the emission of ^{11}B, the minimum potential energy corresponds to both fragments having ratios of major to minor axes equal to about 1.25, which results in a lowering of the Coulomb interaction energy by about ten percent. This is in the right direction but not of a large enough magnitude to account for the low values of the fitted Coulomb barriers. However, another feature of the potential energy surface is its shallowness. That is, only two MeV in the deformation coordinates produces a spread of ten MeV in the Coulomb interaction energy and consequently in the final kinetic energies of the separated fragments.[59,60] Thus it is possible that a reasonable temperature, say 6 MeV, could produce a large enough variation in deformations to explain part of the widths of the experimental spectra. Then, possibly, it would not be necessary to use such high temperatures (10-13 MeV) to fit the remaining widths of the peaks. It should be noted that the sum of the effective Coulomb barrier and the temperature is essentially determined by

the position of the peak in the experimental spectrum. Thus a lowering of the temperature would raise the effective barrier, and possibly bring it into closer agreement with predictions.

It is also possible that some of the fragments observed here come from the neck of a fissioning nucleus and fall into the classes of light particles from fission or triple fission. Although high energy fission has been studied both with track detectors[61] and semiconductor detectors,[62] this possibility remains undetermined at the moment. It would be desirable to do a coincidence experiment with semiconductor counters to find out what are the partners of the fragments observed here.

B. Suggestions for Further Analyses

Another approach to the analysis of the present data which has more physical content than the curve fitting described above would be a detailed comparison of our double differential cross sections with the results of the following calculation. One would start with Monte Carlo knock-on cascade calculations for the interaction of the incident proton with the uranium nucleus, and then treat the fragments as being evaporated from the excited residues of the knock-on cascade. It would not be sufficient to perform the evaporation part of the calculation only from "typical" excited nuclei, because aspects of the knock-on cascade are reflected in the data, i.e., the unusual characteristics of the neutron-deficient nuclei. Therefore one should take the individual residual nuclei of the knock-on cascade with their deposition momentum and calculate their de-excitation by evaporation with the inclusion of the possible evaporation of all the nuclei studied here. Because of the necessity of keeping track of the double differential

cross sections of so many nuclei, it is clear that a combination of Monte Carlo and analytical methods would have to be used. Because of the computer time involved in such a calculation it would probably be wise to start with a Coulomb-shifted Maxwellian energy spectra and then to consider adding the following improvements: realistic inverse cross sections, liquid-drop distortions, pre-equilibrium evaporation, secondary evaporation, fission competition, and angular momentum. An ultimate aim of these calculations would be to find those aspects of the data which do not at all fall within the framework of this cascade-evaporation model and therefore indicate a more direct process. In this respect the evaporation calculation would be considered as a phase-space calculation and deviations from phase-space behavior would be searched for.

C. Secondary Reactions

It is well known that light fragments produced in high-energy reactions have kinetic energies sufficient to induce secondary reactions in the target. Evidence for the occurrence of such reactions is provided by the radiochemical identification of products with atomic number greater than any possible from the capture of the projectile by the target nucleus. Examples are the indentification of thallium and lead radionuclides in gold targets[63] and the identification of astatine isotopes in lead targets[64] bombarded with protons. Most such studies have involved only the light fragments, helium and lithium.

Our data are interesting in this context because a significant fraction of the energy spectrum of every fragment studied up through argon (element 18) lies above the minimum required for a secondary reaction on uranium. It is clear that a variety of such reactions must occur. Our data also show that many of

the fragments are quite rich in neutrons[65] so that in effect heavy element targets bombarded with GeV protons supply a source of high energy projectiles of a type not available in conventional accelerators.[66] Although the fluxes are quite low it is possible that some exotic nuclei could be prepared with the aid of such secondary reactions.

An interesting possibility occurs in the super-heavy elements where theory[67,68] suggests rather strongly that nuclei with atomic numbers near 114 and neutron number near 184 may have half lives of months, years, or longer. It is possible that one could prepare for identification enough atoms of such interesting nuclei by a long bombardment of a large sample (grams to kilograms) of uranium, plutonium, or curium with GeV protons. The beam stop of the accelerator might be the appropriate location for such a target.

Because of the lack of data for fragments beyond argon and for the pertinent secondary reaction cross sections it is impossible to make order-of-magnitude estimates of the yields of such products. In lieu of this it may be useful for purposes of orientation to estimate the yield for a simpler reaction. We consider the case of the secondary reaction $^{238}U(^{14}C,4n)^{248}Cf$ and start by assuming that it has an excitation function similar to that reported by Sikkeland et al.[69] for the reaction $^{238}U(^{12}C,4n)^{246}Cf$; (maximum yield of 0.6 mb at a ^{12}C energy of 68 MeV). We estimate the total yield of ^{14}C with energy sufficient to induce this reaction to be 2 mb in the case of the irradiation of uranium with 5.5-GeV protons. The effective target thickness for the secondary reaction can be estimated from range-energy calculations for ^{14}C to be 10 mg/cm^2. If we assume a 24-gm/cm^2 block of uranium bombarded with a flux of 5×10^{12} protons per minute until half saturation of the ^{248}Cf yield (1 year bombardment) the total number

of ^{248}Cf atoms in the target is about 3×10^6. Yields of products far above californium will of course be substantially lower but perhaps still within a useful range.

ACKNOWLEDGMENTS

We would like to thank the many people who have contributed in numerous ways to these experiments. For our initiation into the world of particle identification we are especially indebted to the guidance and advice of Joseph Cerny and Sam Cosper. For the design of our electronic equipment and invaluable help in solving our problems we especially thank Frederick Goulding and Donald Landis. We are indebted for the semiconductor counters to R. Lothrop, M. Roach, and H. Sommer, for the design of the scattering chamber to R. Burton, and for the UF_4 target to G. Steers. Several different computer programs for calculating range-energy were used in the course of this work and for their use we would like to thank C. Maples, H. Bichsel, and P. Steward. The computer system was contributed to by many people, among them S. Andreae, D. Fanshier, J. Hunter, F. Kirsten, T. Taussig, L. Robinson, and R. Zane. However, the two people who deserve the most credit for the computer system are John Meng and David Jenson. Greatly appreciated was the outstanding hospitality of the Bevatron staff including T. Elioff, F. Lothrop, W. Olson, K. Crebbin, G. White, and H. Ellison. We wish to thank J. B. Cumming for checking the accuracy of our curve-calculating program used in the discussion section. We also appreciate discussions of our results with S. Bjørnholm, I. Dostrovsky, Z. Fraenkel, and W. Swiatecki.

APPENDIX

Cross sections for ^{7}Be production in the interaction of 5.5-GeV protons with uranium, silver, and aluminum, and for ^{22}Na production from aluminum.

As mentioned in the text all cross section measurements made in this study were computed relative to the alpha-particle counting rate in a monitor telescope and were converted to an absolute basis by the use of a cross section for ^{7}Be production determined by a radiochemical method. The radiochemical determination is described here. Although there were previous measurements of the cross section for production of ^{7}Be from U in the literature, the recent measurements[35] were not at the present irradiation energy and interpolation appeared to be too uncertain (see Table I). Also because of the considerable fraction of the ^{7}Be spectrum with high energy, as shown in Fig. 9, it was thought that the previous measurements[32,35] were low because of recoil loss from the relatively thin targets that were used.

In brief the method consisted of the bombardment of aligned stacks of polystyrene and uranium foils, the measurement of the relative number of ^{7}Be nuclei produced in these foils, and the computation of the ^{7}Be cross section in uranium on the basis of the ^{7}Be formation cross section in carbon as determined from previously reported work.[70,71] Because we were in need of a similar cross section reference in measurements of fragments from silver and aluminum targets to be reported elsewhere, we included foils of these elements in our foil stack and simultaneously determined the ^{7}Be formation cross section in silver and aluminum. In the case of aluminum we also determined the ^{22}Na formation cross section. Results are given in Table VI. Experimental details are given below. A general discussion of foil activation techniques and associated errors is given in the review article by Cumming.[70]

Foil Stacks and Irradiation Details

Each of four activation runs was done with a stack of rectangular foils with dimensions 1.25 × 2.55 cm. The beam entered the foil stack at right angles and passed through three foils of each element in the order C (polystyrene), Al, Ag, and U. Each foil was weighed separately; the foil thicknesses varied slightly about the following values: 12.4 mg/cm^2 polystyrene, 21.7 mg/cm^2 Al, 185 mg/cm^2 Ag, and 500 mg/cm^2 U. Only the center foil of each set of three was used for activity measurements; the outer foils protected the center foils and also provided ^{7}Be nuclei to compensate for those lost by recoil. The purity of the polystyrene, Al and Ag foils was > 99%. The polystyrene was assumed to have the chemical composition $(CH)_n$. The uranium metal sheet was pickled in dilute HCl before cutting and weighing in order to remove oxide scale. Errors in the determination of foil thickness were: polystyrene (3%), Al (2%), Ag (2%), and U (3%).

The foil stack was fastened with tape to the upstream side of a 0.003-inch aluminum sheet attached to the standard target frame in the center of our chamber. The alignment of the foils was accurate to 1 mm but this alignment was not critical because the beam was distributed over about two thirds of the foil area, as determined by radioautographs made after the bombardments. The bombardment periods were eight hours at a beam intensity of 5 × 10^{12} protons per minute.

Chemical Procedure for Isolation of ^{7}Be from U

This procedure was adapted from those described elsewhere.[72,73] A standard solution of Be carrier was made by dissolving ultra-pure Be metal in HCl and

diluting to make a solution containing 4.80 mg Be/ml. The uranium foil was dissolved in an $HCl-HNO_3$ mixture and a one ml aliquot of Be standard solution was added. Uranium was removed from the solution by absorption on Dowex A1 resin from 10 M HCl. Beryllium was precipitated as $Be(OH)_2$, dissolved in dilute acid, absorbed on a column of Dowex 50 resin, washed with water, desorbed with 1.5 M HCl and finally precipitated as $BaBeF_4$ by addition of HF and a solution of $Ba(NO_3)_2$. The precipitate was filtered as a thin circular deposit of 1 cm diameter onto a weighed RA-type Millipore filter and weighed to determine an interim chemical yield. The yields averaged 80%. After completion of the ^7Be counting the $BaBeF_4$ precipitate was dissolved and analyzed for beryllium by a spectrophotometric method using the reagent 2-phenoxyquinizarin-3-4'-disulfonic acid.[73,74] The more accurate final values for samples from bombardments 2 and 3 were 8% lower than the interim yields determined by weighing of $BaBeF_4$. The determination of the first sample by the spectrophotometric method was faulty and the interim value was used with an 8% downward adjustment. The uranium foil from the fourth irradiation was not processed. The estimated error in the Be analysis was 3% random and 3% systematic.

Chemical Procedure for Isolation of ^7Be from Ag

The silver foil was dissolved in HNO_3 with the assistance of $NaNO_2$ catalyst. One ml of the standard Be solution was converted from dilute HCl to dilute HNO_3 and added to the Ag solution. $Be(OH)_2$ was precipitated with NH_4OH, washed, dissolved, and reprecipitated. This precipitate was dissolved in concentrated HCl. From this point on the procedure was identical with that described for the uranium targets starting with the anion-exchange resin step. The chemical yields averaged 60%.

^{7}Be and ^{22}Na Radioactivity Measurements

The $BaBeF_4$ precipitates on Millipore filter paper were wrapped in a thin Mylar sheet and affixed with tape to the center of a 1.5 mm thick aluminum counting plate under a 2 mm thick aluminum disc. The polystyrene and aluminum foils were similarly mounted without chemical processing. The counting plates could be positioned in a reproducible geometry 4.9 cm from the front surface of a planar Ge(Li) semiconductor detector. The detector had a depletion thickness of 13 mm and had 8 cm^3 of sensitive volume. The gamma spectrum of each sample was measured and the intensity of the photopeak of the 478-keV ^{7}Be gamma-ray was computed. In the case of the Al target the intensity of the 511-keV annihilation quanta was also measured. The counting rate in these peaks 18-25 days after the bombardment ranged from 5 to 45 counts per minute. All counts were corrected for the 53.6-day ^{7}Be half life. Counting errors were 1.3% or less in all cases except for ^{7}Be and ^{22}Na from Al where they were 2%.

Computation of ^{7}Be Cross Sections and Estimation of Errors

The ^{7}Be produced in the polystyrene was used as the beam monitor under the assumption of a 9.45-mb cross section, which is an interpolated value obtained from a plot of the values determined by Stehney and Steinberg[71] for protons of 3 to 12 GeV and those summarized by Cumming[70] for lower and higher proton energies. The absolute error in this monitor cross section is 8%. The cross section calculation for ^{7}Be from U and Ag involves the foil thicknesses, the chemical yields, and the ^{7}Be activity rates (sample versus monitor). No determination of absolute counting efficiency was necessary. The ^{7}Be cross section in Al was computed in the same way except that no chemical yield correction was needed.

The random error expected from uncertainties in foil thickness, chemical yield, and counting rates amounted to 5.3% for the U and Ag sets, which is to be compared with the observed standard deviation of 6.1%. We selected the larger of these two numbers, divided by the square root of the number of determinations, and combined this with the 3% systematic error in the chemical yield to obtain a value of 4.6% for the total standard error of the measured cross section relative to the monitor. When the 8% error in the monitor cross section was included the absolute error rose to 9.2%. The cross sections and errors are summarized in mb in Table VI.

In the Al set no chemical yield was involved and the expected random error was 4.3% compared to an observed standard deviation of 4.1%. Division of the 4.3% value by the square root of the number of determinations resulted in 2.2% for the standard error. Inclusion of the monitor error raised the absolute error to 8.3%

We also considered the possibility that secondary reactions in our rather thick foil stacks might have contributed to the observed ^{7}Be. Basing our estimates on the discussion given by Cumming[70] and the data published by Stehney and Steinberg[75] we conclude that this effect is negligible.

Computation of ^{22}Na Cross Section in Al

In this case no chemical yield was involved but it was necessary to make decay scheme corrections and to know the relative counting efficiency of the detector for 478- and 511-keV radiation. For ^{7}Be we used 10.3% as the percentage per disintegration of the 478-keV gamma ray and 53.6 days for the half life. For ^{22}Na we used 179.7% as the percentage per disintegration of the 511-keV

photons and 2.6 years for the half life. In the counting arrangement the ^{22}Na was sandwiched between aluminum plates of sufficient thickness to stop the positrons. The counting efficiency (composed of geometry and detector efficiency) was determined as a function of photon energy with the aid of ^{137}Cs, ^{22}Na, ^{54}Mn, and ^{203}Hg standards obtained from the International Atomic Energy Agency. The efficiency for the 478-keV gamma ray of ^{7}Be was 9.3×10^{-4} and for 511-keV photons was 8.7×10^{-4}. Only the error of these values relative to each other is significant for our measurements and it is estimated to be < 1%. Random errors expected from counting statistics and foil thicknesses totaled 4.3% to be compared with 4.6% for the observed standard error. Division of the 4.6% value by the square root of the number of determinations and allowing for a 1% systematic error leads to a standard error of 2.5%. When the 8% error in the monitor is included this increases to 8.4%.

Acknowledgment

We thank Mrs. Ursula Abed for the analysis of the Be samples by the colorimetric method.

FOOTNOTES AND REFERENCES

*Work performed under the auspices of the U. S. Atomic Energy Commission.

†Present address: Chemistry Division, Argonne National Lab., Argonne, Illinois 60439.

1. A. M. Poskanzer, S. W. Cosper, E. K. Hyde, and J. Cerny, Phys. Rev. Letters 17, 1271 (1966).

2. A. M. Poskanzer, G. W. Butler, E. K. Hyde, J. Cerny, D. A. Landis, and F. S. Goulding, Phys. Letters 27B, 414 (1968).

3. T. D. Thomas, G. M. Raisbeck, P. Boerstling, G. T. Garvey, and R. P. Lynch, Phys. Letters 27B, 504 (1968).

4. G. M. Raisbeck, P. Boerstling, P. Riesenfeldt, T. D. Thomas, R. Klapisch, and G. T. Garvey, Phys. Letters, to be published (1970).

5. A. G. Artukh, G. F. Gridnev, V. L. Mikheev, and V. V. Volkov, Nucl. Phys. A137, 348 (1969).

6. A. G. Artukh, V. V. Avdeichikov, G. F. Gridnev, V. L. Mikheev, V. V. Volkov, and J. Wilczynski, Phys. Letters 31B, 129 (1970).

7. A. G. Artukh, V. V. Avdeichikov, L. P. Chelnokov, G. F. Gridnev, V. L. Mikheev, V. I. Vakatov, V. V. Volkov, and J. Wilczynski, Phys. Letters 32B, 43 (1970).

8. R. Klapisch, C. Phillipe, J. Suchorzewska, C. Detraz, and R. Bernas, Phys. Rev. Letters 20, 740 (1968).

9. R. Klapisch, C. Thibault, C. Detraz, J. Chaumont, R. Bernas, and E. Beck, Phys. Rev. Letters 23, 652 (1969).

10. G. Friedlander, "Fission of Heavy Elements by High Energy Protons," in Physics and Chemistry of Fission, (International Atomic Energy Agency, Vienna, 1965), Vol. II, p. 265.

11. B. D. Pate and A. M. Poskanzer, Phys. Rev. 123, 647 (1961).

12. For a general review of high-energy reaction phenomena and interpretation see J. Hudis, Chapter 3 in Nuclear Chemistry Vol. I, L. Yaffe, Editor,

(Academic Press, New York, 1968). There exists also an earlier general review by J. M. Miller and J. Hudis, Ann. Rev. Nucl. Sci. 9, 159 (1959). E. K. Hyde has reviewed high energy reactions with an emphasis of fission in the book "Fission Phenomena," Vol. III in the series on The Nuclear Properties of the Heavy Elements, (Prentice Hall, Inc., Englewood Cliffs, New Jersey, 1964).

13. A review of the application of recoil technique to a determination of reaction mechanisms is given by J. M. Alexander, Chapter 4 in Nuclear Chemistry, Vol. I, L. Yaffe, Editor, (Academic Press, New York, 1968).

14. R. Wolfgang, E. W. Baker, A. A. Caretto, J. B. Cumming, G. Friedlander, and J. Hudis, Phys. Rev. 103, 394 (1956).

15. General review of the fragment literature including much data obtained by nuclear emulsion techniques is given by the following authors: N. A. Perfilov, O. V. Lozhkin, and V. P. Shamov, Usp. Fiz. Nauk 60, 3 (1960) [English trans. Soviet Phys.--Usp. 3, 1 (1960)]; N. A. Perfilov, O. V. Lozhkin, and V. I. Ostroumov, Nuclear Reactions Induced by High-Energy Particles, Moscow (1962) in Russian [English Trans. unpublished Lawrence Radiation Laboratory Report UCRL-Trans. 949 (1963)]; M. Lefort, Ann. Phys. 9, 249 (1964); M. Lefort and G. N. Simonoff, Journal de Physique 29, C1, 25 (1968). A short review is given in the introduction to Ref. 16.

16. V. P. Crespo, J. M. Alexander, and E. K. Hyde, Phys. Rev. 131, 1765 (1963).

17. J. B. Cumming, R. J. Cross, Jr., J. Hudis, and A. M. Poskanzer, Phys. Rev. 134, B167 (1964).

18. J. Hudis and J. M. Miller, Phys. Rev. 112, 1322 (1958).

19. I. Dostrovsky, Z. Fraenkel, and P. Rabinowitz, Phys. Rev. 118, 791 (1960).

20. I. Dostrovsky, Z. Fraenkel, and J. Hudis, Phys. Rev. 123, 1452 (1961).

21. I. Dostrovsky, R. Davis, Jr., A. M. Poskanzer, and P. L. Reeder, Phys. Rev. 139, B1513 (1965).

22. V. P. Crespo, J. B. Cumming, and A. M. Poskanzer, Phys. Rev. 174, 1455 (1968).

23. V. P. Crespo, J. B. Cumming, and J.M. Alexander, Phys. Rev. to be published (1970).

24. S. Katcoff, E. W. Baker, and N. T. Porile, Phys. Rev. 140, B1549 (1965).

25. E. L. Grigor'ev, O. V. Lozhkin, V. M. Mal'tsev, and Yu. P. Yakovlev, Sov. J. Nucl. Phys. 6, 507 (1968).

26. G. D. Harp, J. M. Miller, and B. J. Berne, Phys. Rev. 165, 1166 (1968).

27. J. J. Griffin, Phys. Rev. Letters 17, 478 (1966); Phys. Letters 24B, 5 (1967).

28. M. Blann, Phys. Rev. Letters 21, 1357 (1968); M. Blann and F. M. Lanzafame, Nucl. Phys. A142, 559 (1970).

29. F. C. Williams, Jr., Phys. Letters 31B, 184 (1970).

30. F. S. Goulding, D. A. Landis, J. Cerny III, and R. H. Pehl, Nucl. Instr. Methods 31, 1 (1964).

31. W. F. Fry, Ann. Rev. Nucl. Sci. 8, 105 (1958).

32. C. L. Carnahan, Lawrence Radiation Laboratory Report UCRL-8020, 1957, (unpublished).

33. A. A. Caretto, J. Hudis, and G. Friedlander, Phys. Rev. 110, 1130 (1958).

34. A. Juliano and N. T. Porile, J. Inorg. Nucl. Chem. 29, 2859 (1967).

35. J. Hudis and S. Tanaka, Phys. Rev. 171, 1297 (1968).

36. J. Hudis, Phys. Rev. 171, 1301 (1968).

37. J. Hudis, T. Kirsten, R. W. Stoenner, and O. A. Schaeffer, Phys. Rev. C 1, 2019 (1970). Also J. Hudis, private communication (1970).

38. S. Katcoff, Phys. Rev. 114, 905 (1959).

39. W. Gajewski, P. A. Gorichev, and N. A. Perfilov, Nucl. Phys. 69, 445 (1965).

40. P. A. Gorichev, O. V. Lozhkin, and N. A. Perfilov, Sov. J. Nucl. Phys. 5, 19 (1967).

41. S. W. Cosper, J. Cerny, and R. C. Gatti, Phys. Rev. 154, 1193 (1967).

42. G. M. Raisbeck and T. D. Thomas, Phys. Rev. 172, 1272 (1968).

43. A review has been given by N. Feather, in Proceedings of the Second Symposium on Physics and Chemistry of Fission, (IAEA, Vienna, 1969), p. 83.

44. More recent references are contained in Y. Gazit, E. Nardi, and S. Katcoff, Phys. Rev. C 1, 2101 (1970).

45. F. S. Goulding, D. A. Landis, J. Cerny, and R. H. Pehl, IEEE Trans. Nucl. Sci. 13, 514 (1966).

46. J. Cerny, S. W. Cosper, G. W. Butler, H. Brunnader, R. L. McGrath, and F. S. Goulding, Nucl Instr. Methods 45, 337 (1966).

47. G. W. Butler, J. Cerny, S. W. Cosper, and R. L. McGrath, Phys. Rev. 166, 1096 (1968).

48. C. C. Maples, Jr., and J. Cerny, personal communication.

49. P. G. Steward, University of California Lawrence Radiation Laboratory Report UCRL-18127, 1968, (unpublished).

50. R. H. Pehl, F. S. Goulding, D. A. Landis, and M. Lenzlinger, Nucl. Instr. Methods 59, 45 (1968).

51. L. B. Robinson, F. Gin, and H. Cingolani, Nucl. Instr. Methods, to be published (1970).

52. L. B. Robinson, F. Gin, and F. S. Goulding, Nucl. Instr. Methods 62, 237 (1968).

53. D. W. Jenson, Lawrence Radiation Laboratory Report UCRL-19402, 1969, (unpublished).

54. H. Bichsel and C. Tschalaer, Nucl. Data A3, 343 (1967).

55. This was done as just described for the other estimates, but by the use of the relative yields at 90° at 90 MeV from Fig. 12 for determining the trend of the experimental bias, and then normalizing the sum of the yields to the total nitrogen cross section obtained from the element energy spectra as described later in the text.

56. When you calculate this quantity from $(\langle k \rangle B + \tau)(220 - A)/220$ it comes out somewhat lower because of the effect of the smearing parameter, Δ.

57. R. DaSilveira, Phys. Letters 9, 252 (1964).

58. J. C. D. Milton (1962). Private communication from W. J. Swiatecki (1970).

59. J. R. Nix and W. J. Swiatecki, Nucl. Phys. 71, 1 (1965).

60. T. D. Thomas, W. M. Gibson, and G. J. Safford, Physics and Chemistry of Fission, (International Atomic Energy Agency, Vienna, 1965), Vol. II, p. 467.

61. J. Hudis and S. Katcoff, Phys. Rev. 180, 1122 (1969); G. Remy, J. Ralarosy, R. Stein, M. Debeauvais, and J. Tripier, Journal de Physique 31, 27 (1970).

62. L. P. Remsberg, F. Plasil, J. B. Cumming, and M. L. Perlman, Phys. Rev. 187, 1597 (1969).

63. A. E. Metzger and J. M. Miller, Phys. Rev. 113, 1125 (1959).

64. M. Lefort and X. Tarrago, Nucl. Phys. 46, 161 (1963).

65. See also Ref. 9.

66. An exception is reported by E. Cheifetz, R. C. Gatti, R. C. Jared, S. G. Thompson, and A. Wittkower, Phys. Rev. Letters 24, 148 (1970).

67. V. M. Strutinsky, Nucl. Phys. A95, 420 (1967); and A122, 1 (1968).

68. S. G. Nilsson, C. F. Tsang, A. Sobiczewski, Z. Szymanski, S. Wycech, C. Gustafson, I. L. Lamm, P. Möller and B. Nilsson, Nucl. Phys. A131, 1 (1969).

69. T. Sikkeland, J. Maly, and D. F. Lebeck, Phys. Rev. 169, 1000 (1968).

70. J. B. Cumming, Ann. Rev. Nucl. Sci. 13, 261 (1963).

71. A. F. Stehney and E. P. Steinberg, Nucl. Phys. B5, 188 (1968).

72. A. W. Fairhall, The Radiochemistry of Beryllium, National Academy of Sciences--National Research Council Report NAS-NS 3013, (1960).

73. E. F. Norton, Chemical Yield Determinations in Radiochemistry, National Academy of Sciences--National Research Council Report NAS-NS 3111.

74. E. G. Owens and J. H. Yoe, Anal. Chem. 32, 1345 (1960).

75. A. F. Stehney and E. P. Steinberg, Nucl. Instr. Methods 59, 102 (1968).

Table I. Previous measurements of formation cross sections for light fragments from uranium bombarded with GeV protons.[a]

Product	Proton energy (GeV)	Cross section[b] (mb)	Product	Proton energy (GeV)	cross section[b] (mb)
^{9}Li	1.0	1.7[c]	^{22}Na	3	0.8[d]
	2.8	7.5[c]		5.7	2.0[e]
				10	2.0[d]
^{7}Be	3	7.0[d]		30	2.3[d]
	5.7	12[e]			
	10	20.2[d]	^{20}Ne	3	10[i]
	30	20.2[d]		29	38[i]
^{13}N	1.0	0.024[f]	^{21}Ne	3	10[i]
	1.9	0.067[f]		29	38[i]
	2.9	0.105[f]			
			^{22}Ne	3	10[i]
^{16}C	1.0	0.31[c,g]		29	37[i]
	2.8	1.8[c,g]			
			^{24}Ne	1	0.23[j]
^{17}N	1.0	1.1[c]		2	0.67[j]
	2.8	6.3[c]		3	1.74[j]
^{18}F	1.0	0.13[h]	^{24}Na	1	0.61[h,j](0.38)[j]
	2.0	0.48[h]		2	2.55[h,j](1.88)[j]
	3.0	1.2[h]		3	6.00[d,j](4.26)[j]
	4.5	1.6[h]		3.0	4.7[h]
	5.9	2.6[h]		4.5	9.3[h]
				5.7	10[e]
				5.9	9.7[h]
				10	16.5[d]
				11.6	12.5[k]
				30	16.1[d]
			^{28}Mg	5.7	3.2[e]

(continued)

Table I. Continued

[a]Only fragments below mass 30 are considered.

[b]Cross sections have been normalized to the monitor values given by Cumming.[70]

[c]See Ref. 21.

[d]See Ref. 35.

[e]See Ref. 32.

[f]See Ref. 20.

[g]Lower limit assuming 100% delayed neutron branch.

[h]See Ref. 33.

[i]See Ref. 37. The ^{22}Ne numbers include ^{22}Na.

[j]See Ref. 36. Value in parentheses is independent yield.

[k]See Ref. 34.

Table II. Telescopes used in this study. The numbers given are the thicknesses in microns of the ΔE and E counters, followed in parentheses by the lower discriminator setting in MeV of the E counter.

Target / Isotope	0.7 mg/cm^2 UF_4	10 mg/cm^2 U	28 mg/cm^2 U
^{1-3}H, ^{3}He		61-250(2.2)[a],168-1500(3)	250-5000(5)
^{4}He	20-300(5)[a]	61-250(2.2)[a],168-1500(3)	250-5000(5)
^{6}He	20-300(5)[a]	61-250(2.2)[a]	250-5000(10)
^{8}He			38-195(3),46-38-1000(5)[b]
^{6-8}Li	20-300(5)[a]	61-250(2.2)[a]	250-5000(10)
^{9}Li		61-250(2.2)	250-5000(10)
^{7}Be		20-188(5),61-188(10),100-61-1000(20)[b]	250-5000(10)
$^{9,10}Be$	20-300(5)[a]	20-188(5),61-188(10),100-61-1000(20)[b]	
$^{10-13}B$	20-100(5)[a]	20-188(5),61-188(10),100-61-1000(20)[b]	
$^{11-14}C$	20-100(5)[a]	61-250(10)	
^{15}C, $^{14-17}N$		61-250(10)	
C-Na	20-300(10)		
Na-Ar	20-100(20)		

[a]Blanks measured for the Mylar target backings were subtracted.

[b]Telescopes with two ΔE counters.

Table III. Forward-to-backward ratios and differences. F is the fraction of events going into the forward hemisphere in the laboratory system and B is the fraction in the backward hemisphere.

Isotope	F/B	F-B
^{3}He[a]	1.68	0.25
^{3}He[b]	2.1	0.35
^{4}He	1.24	0.11
^{6}He	1.33	0.14
^{8}He	1.46	0.19
^{6}Li	1.39	0.16
^{7}Li	1.33	0.14
^{8}Li	1.42	0.17
^{9}Li	1.46	0.19
^{7}Be	1.81	0.29
^{9}Be	1.43	0.18
^{10}Be	1.57	0.22
^{10}B	1.61	0.23
^{11}B	1.56	0.22
^{12}B	1.66	0.25
^{13}B	1.70	0.26
^{11}C	2.16	0.37
^{12}C	1.58	0.22
^{13}C	1.56	0.22
^{14}C	1.69	0.26

[a]Has a high energy cutoff of 100 MeV.

[b]A correction has been estimated for the missing parts of the energy spectra above 100 MeV.

Table IV. Total cross sections in mb as a function of mass number (A) and charge number (Z).

A	σ(A)	Z	σ(Z)
2		2	4400
3		3	301
4	3700	4	128
5	0	5	117
6	160	6	96
7	182	7	64
8	53	8	47
9	63	9	35
10	71	10	35
11	79	11	31
12	48		
13	47		
14	≈ 30		

Table V. Parameters obtained from the curve fitting.

	B (MeV)	$\langle k \rangle \pm \Delta$	90° Peak energy (MeV)	τ (MeV)	τ_{HE}^{a} (MeV)	$\langle v \rangle /c$
^{4}He	22	0.58 ± 0.2	20	6	20	0.003
^{6}Li	32	0.57 ± 0.1	29	10	20	0.006
^{7}Li	32	0.58 ± 0.25	31	10	20	0.005
^{7}Be	42	0.44 ± 0.25	38	15	23	0.007
^{10}Be	41	0.48 ± 0.05	33	12	20	0.007
^{11}B	50	0.47 ± 0.10	39	13	19	0.006
C	58	0.45 ± 0.15	42	13	15	0.007
N	66	0.45 ± 0.20	46	13	14	0.006
O	74	0.45 ± 0.20	49	13	14	0.006
F	82	0.45 ± 0.20		13	13	0.005
Ne	89	0.45 ± 0.20		13	13	0.005
Na	96	0.45 ± 0.20		13	13	0.005

[a] τ_{HE} refers to the temperature needed to fit the highest energy part of the 90° spectrum.

Table VI. Formation cross sections for ^{7}Be and ^{22}Na in targets bombarded with 5.5-GeV protons.[a]

Target	σ (mb)	standard error (mb)	standard error[b] (mb)
U (^{7}Be)	17.6	± 0.8	± 1.6
Ag(^{7}Be)	17.4	± 0.8	± 1.6
Al(^{7}Be)	9.2	± 0.2	± 0.8
Al(^{22}Na)	12.2	± 0.3	± 1.0

[a]Relative to $\sigma_C(^{7}Be) = 9.45$ mb.

[b]Including the 8% error in the monitor cross section.

FIGURE CAPTIONS

Fig. 1. Schematic diagram of the detector telescope and the associated electronics.

Fig. 2. Particle spectra from three different experiments at 90° obtained using a telescope containing a 61-μm ΔE detector.

Fig. 3. Particle spectrum resulting from the use of a 20 μm ΔE detector to obtain energy spectra for Na through Ar. For the C through Na data the identifier was optimized for better separation at lower Z.

Fig. 4. Block diagram of the on-line computer system that was used for the collection of the data.

Fig. 5. Experimental data for ^{4}He, ^{7}Li, and ^{10}Be at 90° to the beam showing the smooth curves drawn through the data. The data and curves should be raised by the factor 1.10.

Fig. 6. Laboratory energy spectra at 20°, 45°, 90°, 135°, and 160° to the beam. The five curves are arranged at high energies in decreasing order with increasing angle, except for ^{1}H which is labeled. The dashed lines at low energy indicate the extrapolation used to integrate the energy spectra. All the curves should be raised by the factor 1.10.

Fig. 7. See caption of Fig. 6.

Fig. 8. See caption of Fig. 6.

Fig. 9. See caption of Fig. 6.

Fig. 10. See caption of Fig. 6.

Fig. 11. See caption of Fig. 6.

Fig. 12. See caption of Fig. 6.

Fig. 13. Laboratory energy spectra at 90° to the beam. The curves for each element have been multiplied by a different factor which is indicated in the upper right part of the figure. The broken curves are for the most neutron-deficient isotope of each element. All the curves should be raised by the factor 1.10.

Fig. 14. Laboratory energy spectra at 20°, 90°, and 160° to the beam. The 90° data have been lowered by one decade and the 160° data by two decades. The arrows indicate the low-energy cutoffs for each element. The different broken curves are simply to aid the eye. All the curves should be raised by the factor 1.10.

Fig. 15. Laboratory angular distributions. For ^{1-3}H and ^{3}He the data have high energy cutoffs which are indicated. The curves were drawn by eye and were used to integrate the angular distributions. The points and curves should be raised by the factor 1.10.

Fig. 16. A section of the chart of the nuclides with production cross sections in millibarns indicated for each isotope. These numbers already have been normalized to the value of 17.6 mb for ^{7}Be. The contour lines are for 100, 30, 10, 3, 1, and 0.3 mb. The broken line indicates the bottom of the valley of beta stability.

Fig. 17. Mass yield and charge yield curves. The extensions to A = 15 and Z = 12 are estimated. The dotted curve includes estimates for nuclides without any particle-stable states.

Fig. 18. The ^{11}B data in the laboratory system together with the curves calculated with the following parameters: B = 50 MeV, $\langle k \rangle = 0.47$, $\Delta = 0.10$, $\tau = 13$ MeV, $\langle v \rangle = 0.006$, and n = 2. The curves have been normalized to the data only at the peak of the 90° spectrum. The points and curves have been lowered by one decade at 90° and two decades at 160°.

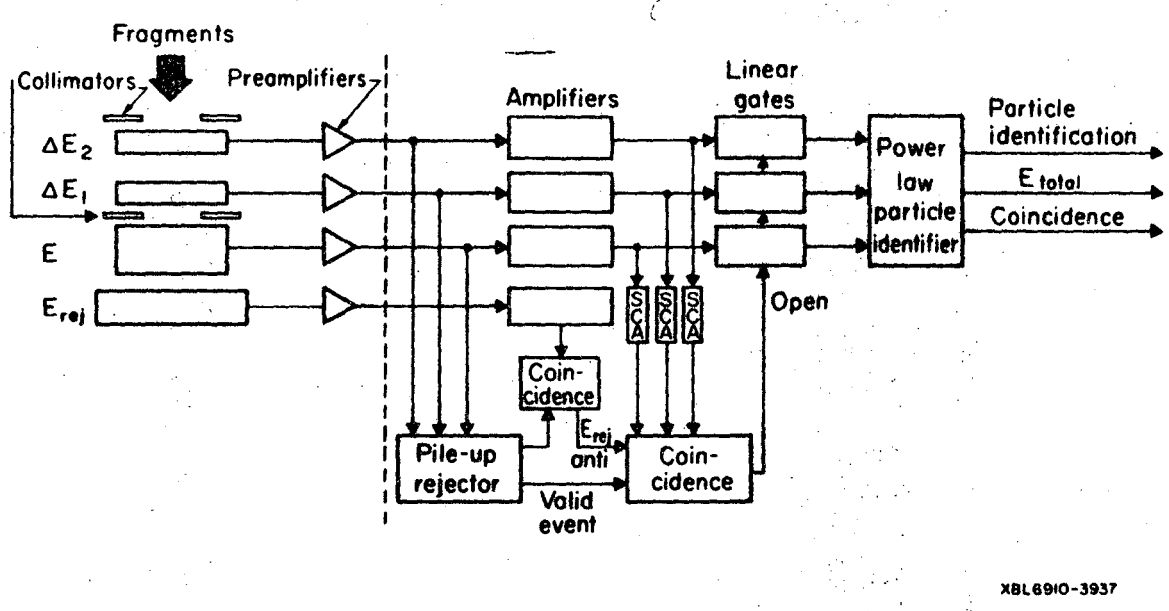
Fragments
Collimators
Preamplifiers
Amplifiers
Linear gates
ΔE2
ΔE1
E
Erej
Power law particle identifier
Particle identification
E total
Coincidence
SCA
SCA
SCA
Open
Coin-cidence
Erej anti
Pile-up rejector
Valid event
Coin-cidence
XBL6910-3937

Fig. 1

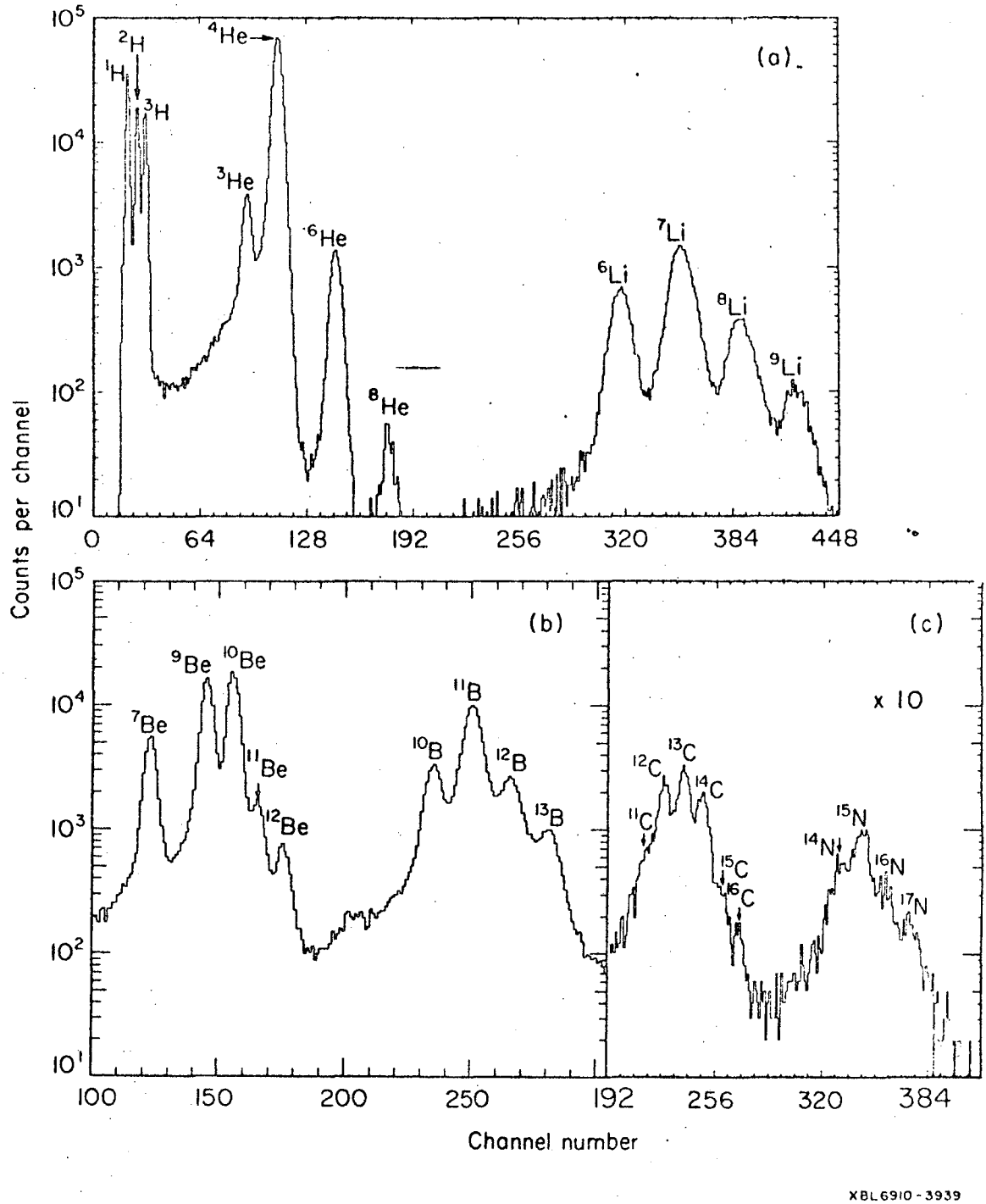

Fig. 2

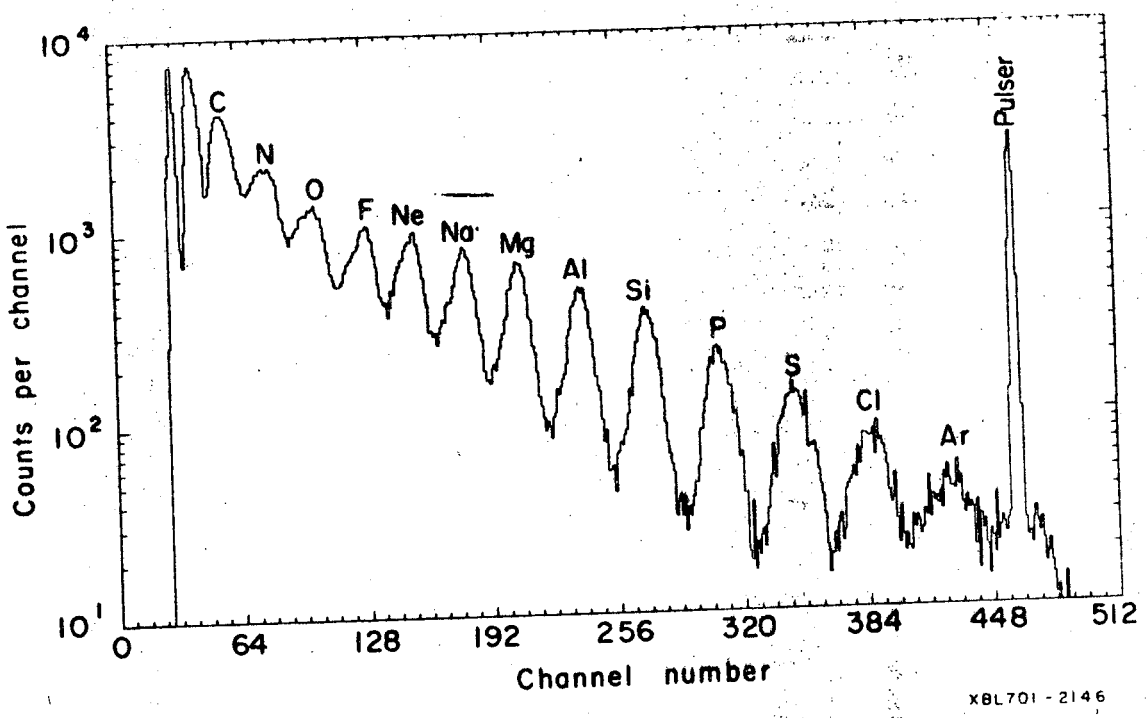
Counts per channel
10^4
10^3
10^2
10^1
C
N
O
F
Ne
Na
Mg
Al
Si
P
S
Cl
Ar
Pulser
0
64
128
192
256
320
384
448
512
Channel number
XBL701-2146

Fig. 3

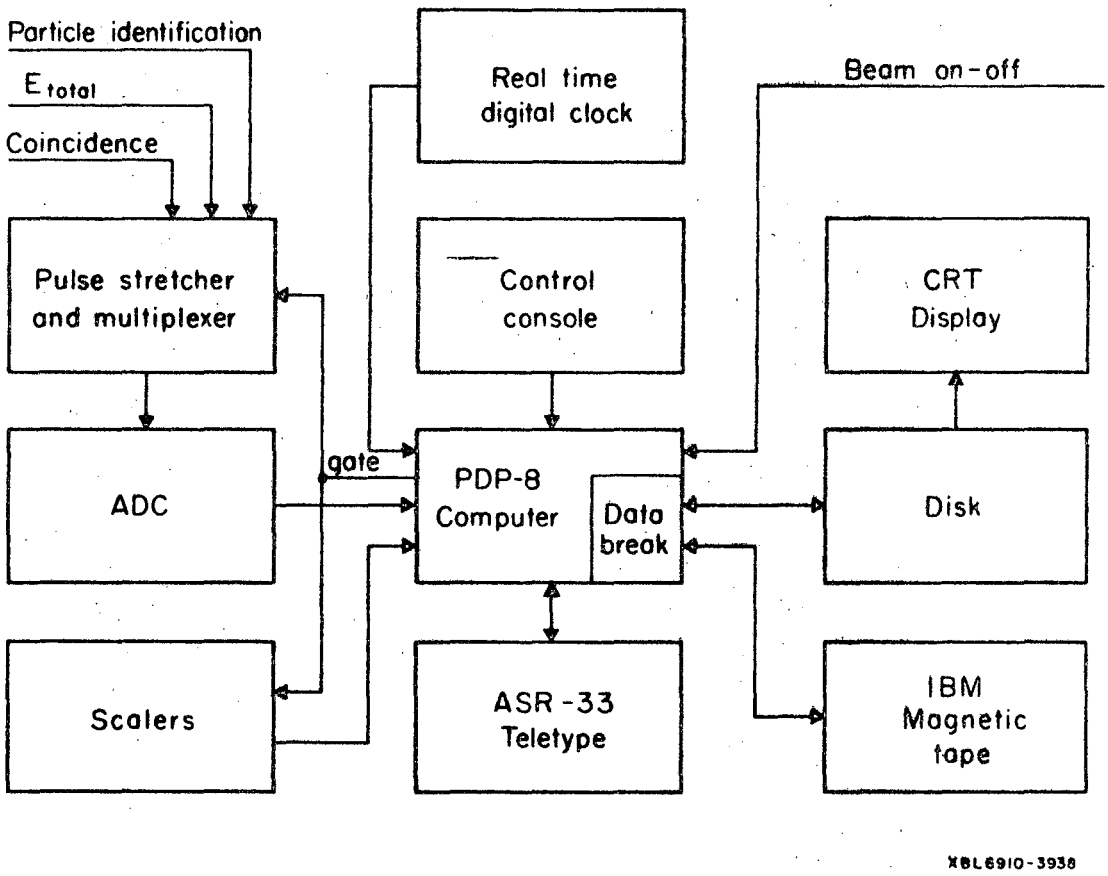
Particle identification
E total
Coincidence
Real time digital clock
Beam on-off
Pulse stretcher and multiplexer
Control console
CRT Display
ADC
gate
PDP-8 Computer
Data break
Disk
Scalers
ASR-33 Teletype
IBM Magnetic tape
XBL6910-3938

Fig. 4

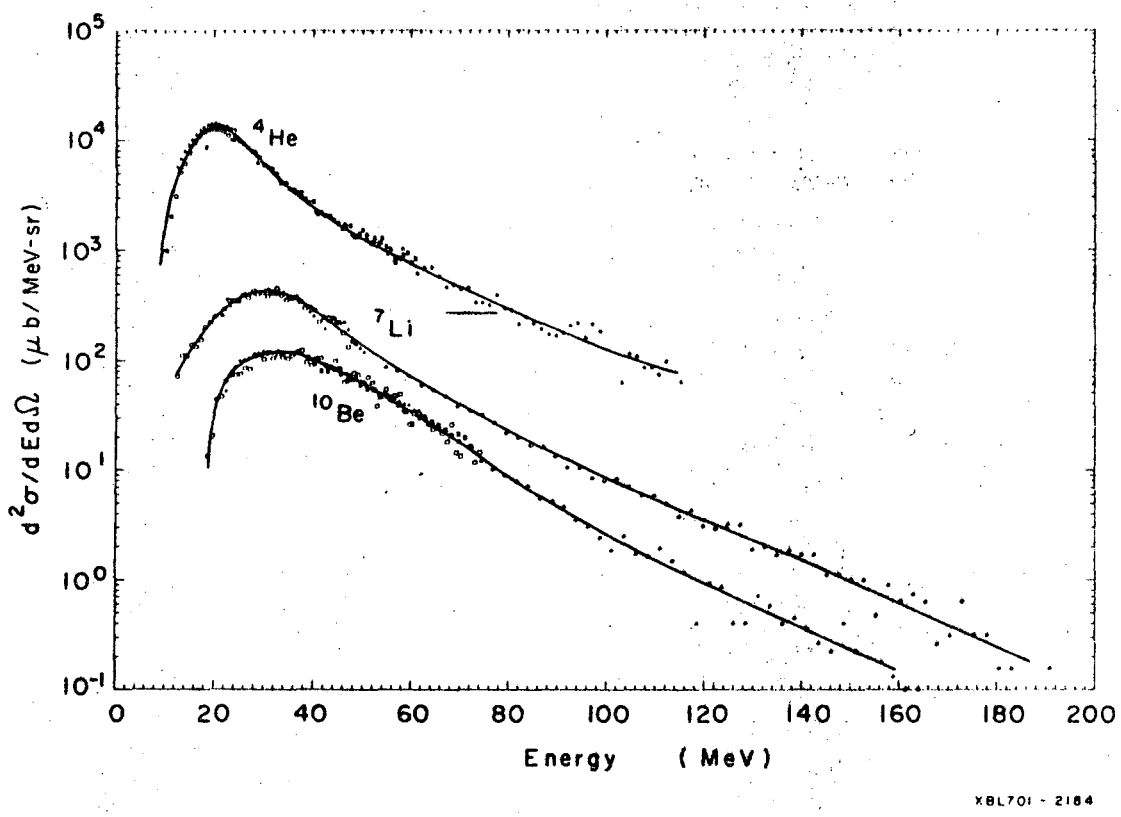
10^5
10^4
10^3
10^2
10^1
10^0
10^{-1}
$d^2\sigma/dEd\Omega$ (μb/MeV-sr)
^{4}He
^{7}Li
^{10}Be
0
20
40
60
80
100
120
140
160
180
200
Energy (MeV)
XBL701 - 2184

Fig. 5

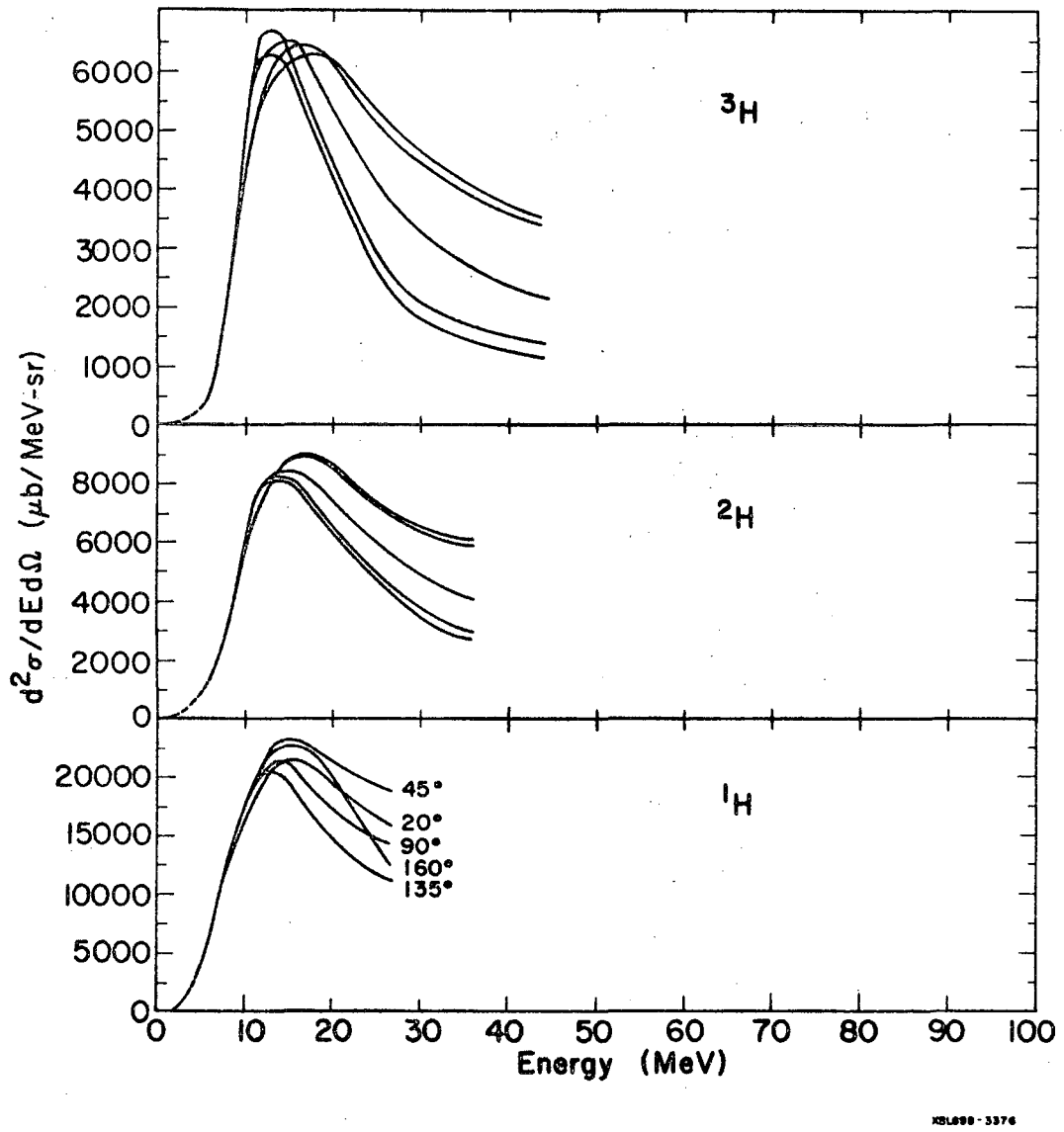
6000
5000
4000
3000
2000
1000
0
^{3}H
8000
6000
4000
2000
0
^{2}H
20000
15000
10000
5000
0
^{1}H
45°
20°
90°
160°
135°
$d^2\sigma/dEd\Omega$ (μb/MeV-sr)
0 10 20 30 40 50 60 70 80 90 100
Energy (MeV)
XBL898-3376

Fig. 6

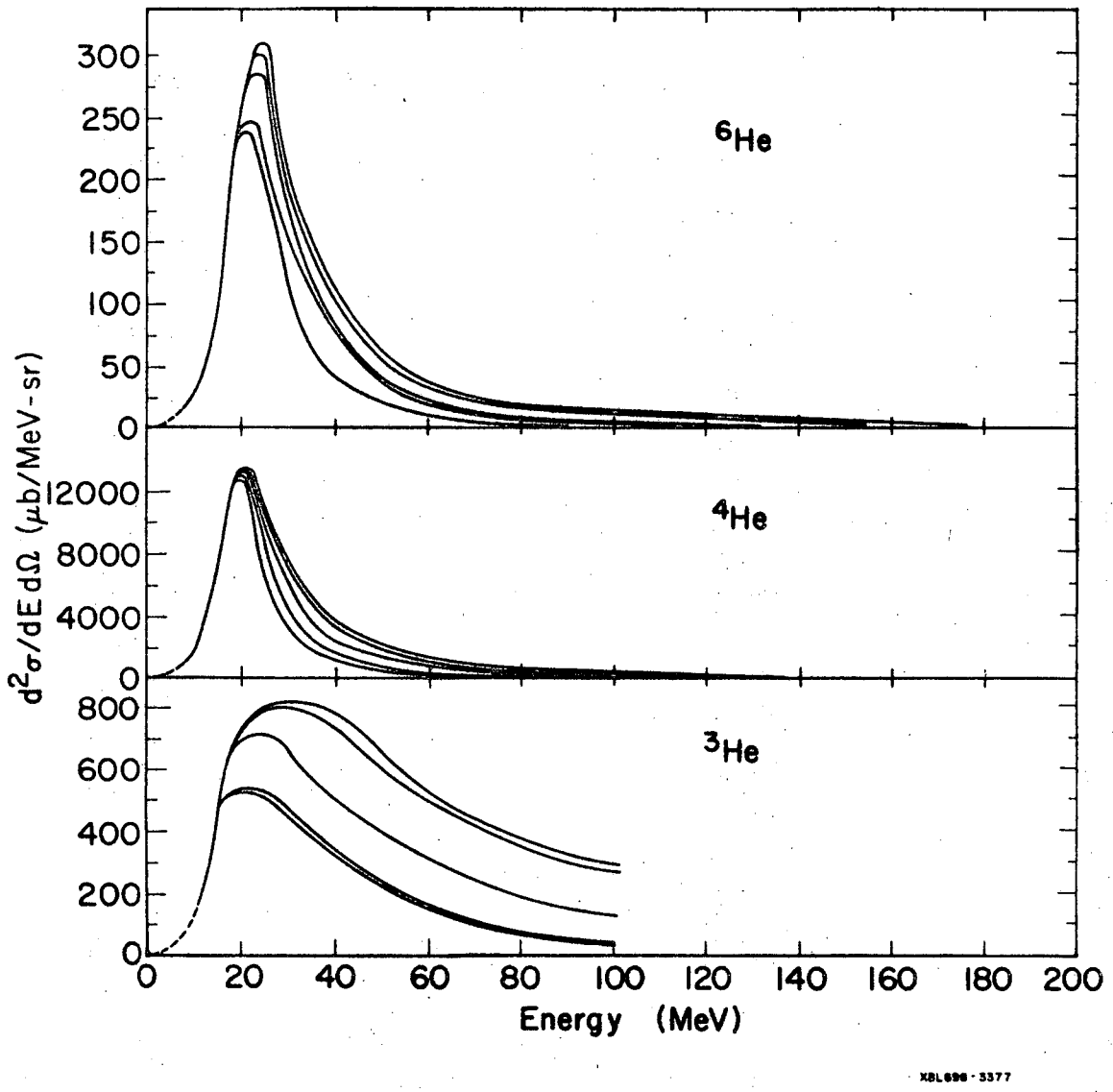
300
250
200
150
100
50
0
^{6}He
12000
8000
4000
0
^{4}He
800
600
400
200
0
^{3}He
$d^2\sigma/dE\,d\Omega$ (μb/MeV-sr)
0
20
40
60
80
100
120
140
160
180
200
Energy (MeV)
XBL696-3377

Fig. 7

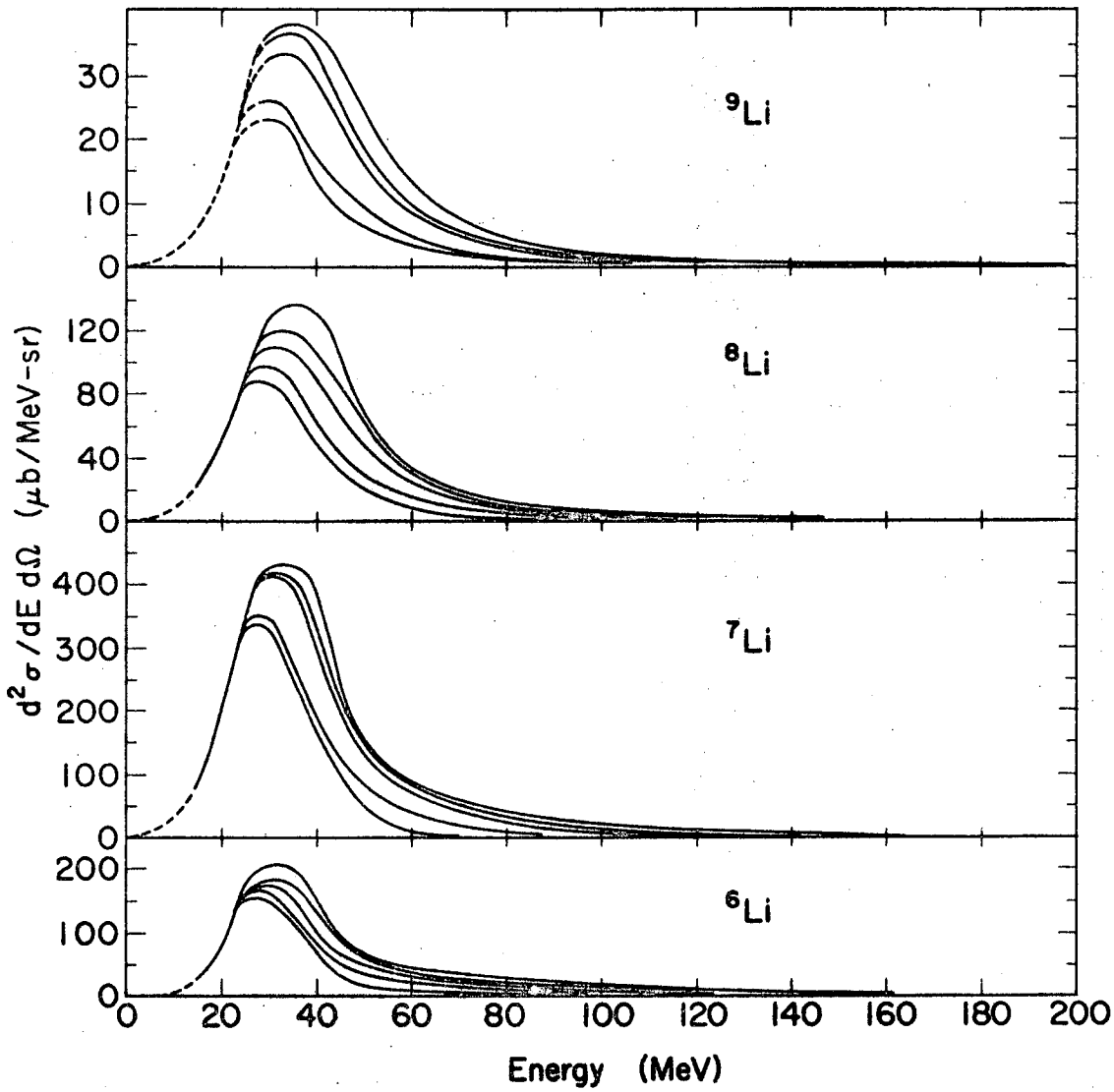

XBL698-3378

Fig. 8

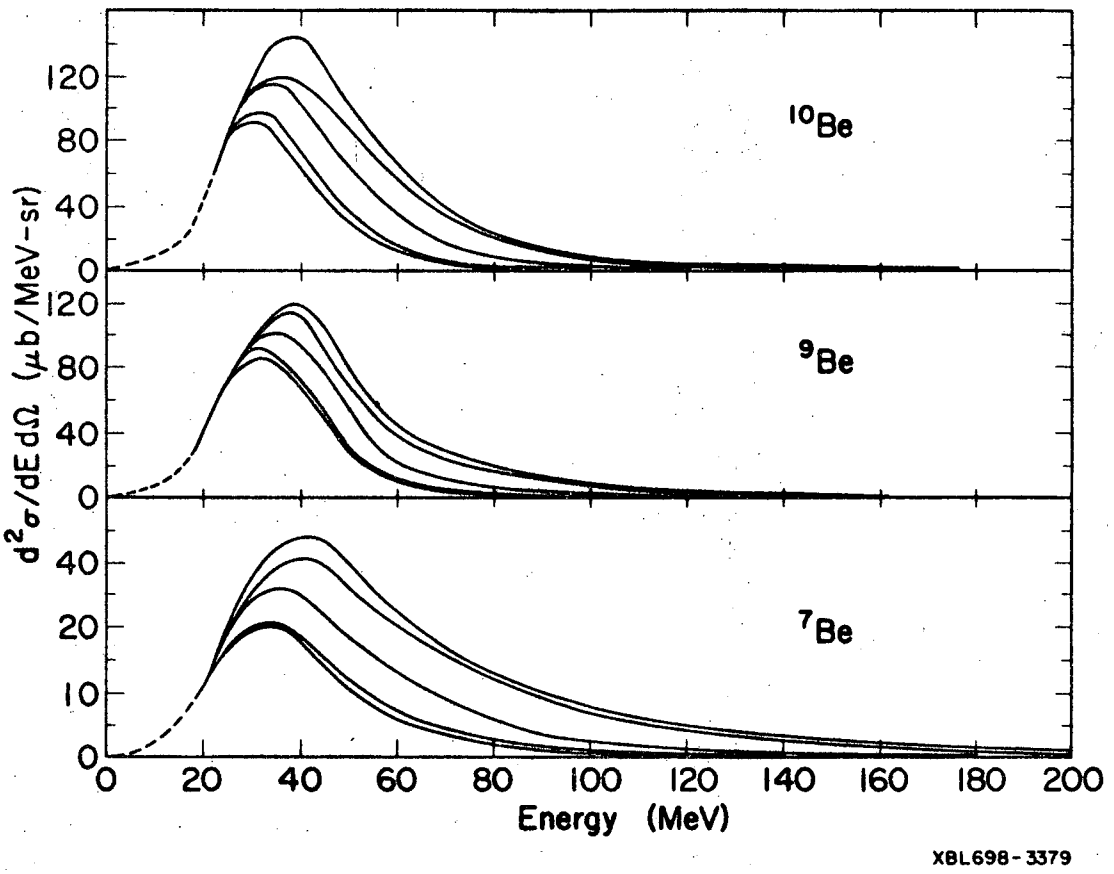
120
80
40
0
120
80
40
0
40
20
10
0
$d^2\sigma/dE\,d\Omega$ (μb/MeV-sr)
^{10}Be
^{9}Be
^{7}Be
0
20
40
60
80
100
120
140
160
180
200
Energy (MeV)
XBL698-3379

Fig. 9

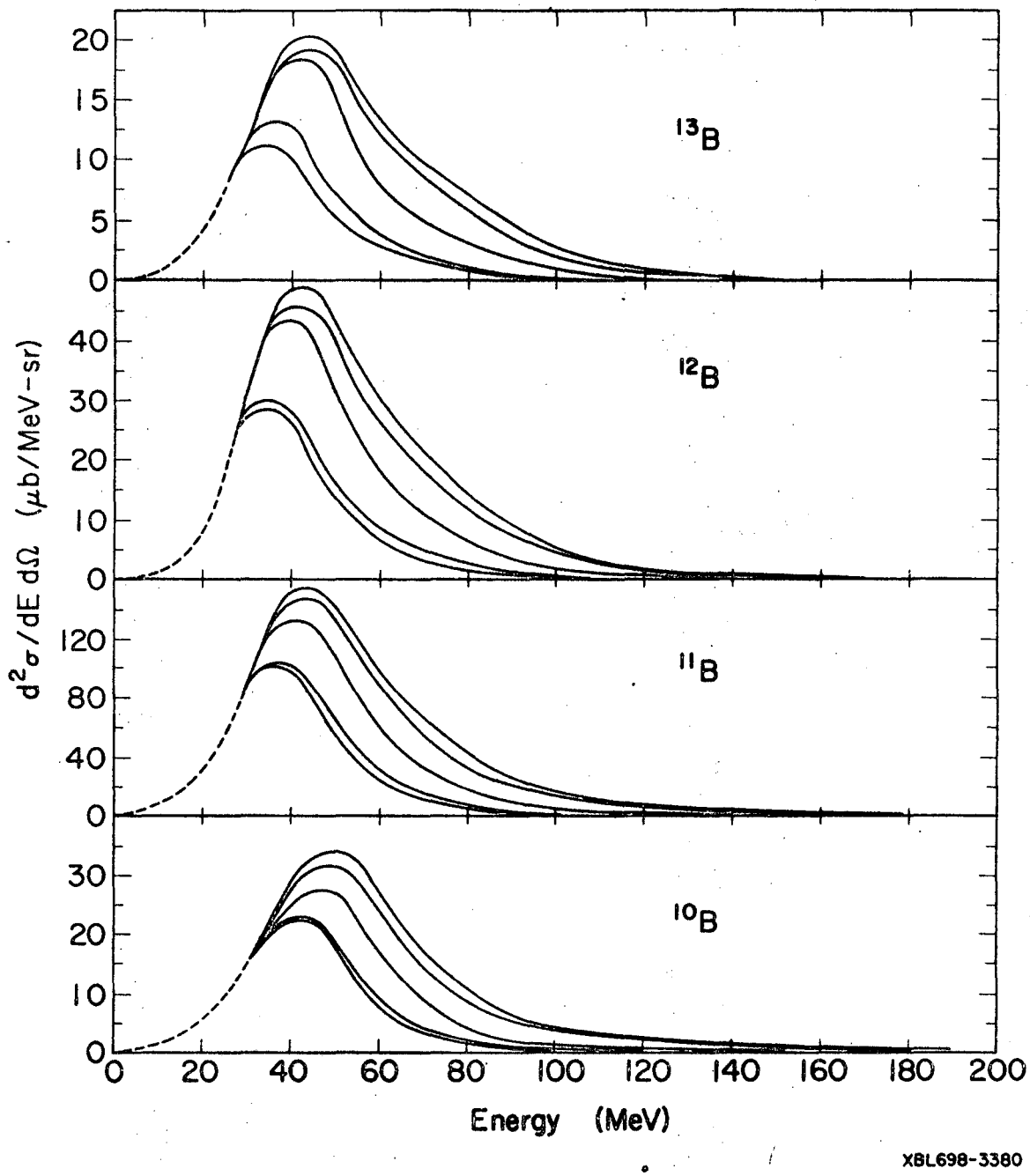
^{13}B
^{12}B
^{11}B
^{10}B
$d^2\sigma/dE\,d\Omega$ (μb/MeV-sr)
Energy (MeV)
XBL698-3380

Fig. 10

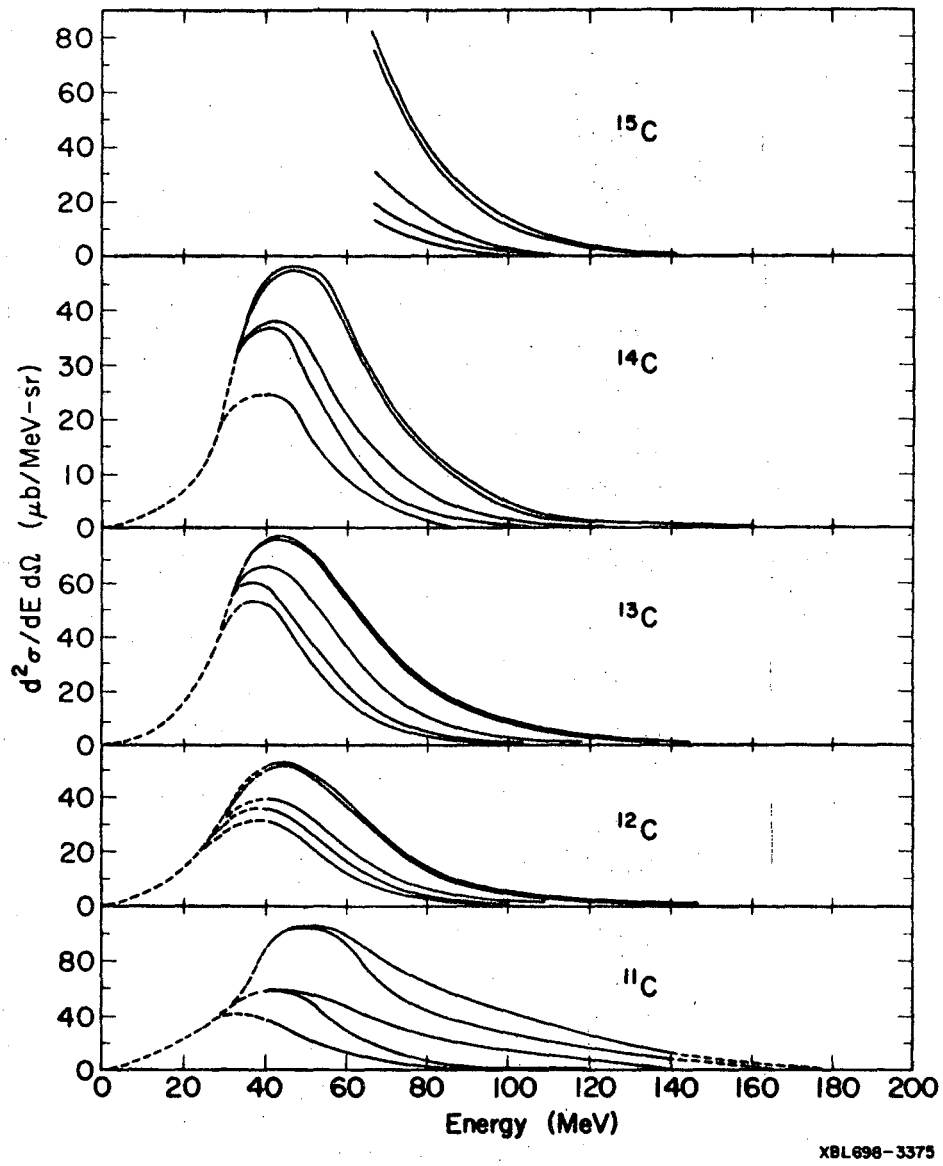
^{15}C
^{14}C
^{13}C
^{12}C
^{11}C
$d^2\sigma/dE\,d\Omega$ (μb/MeV-sr)
Energy (MeV)
XBL698-3375

Fig. 11

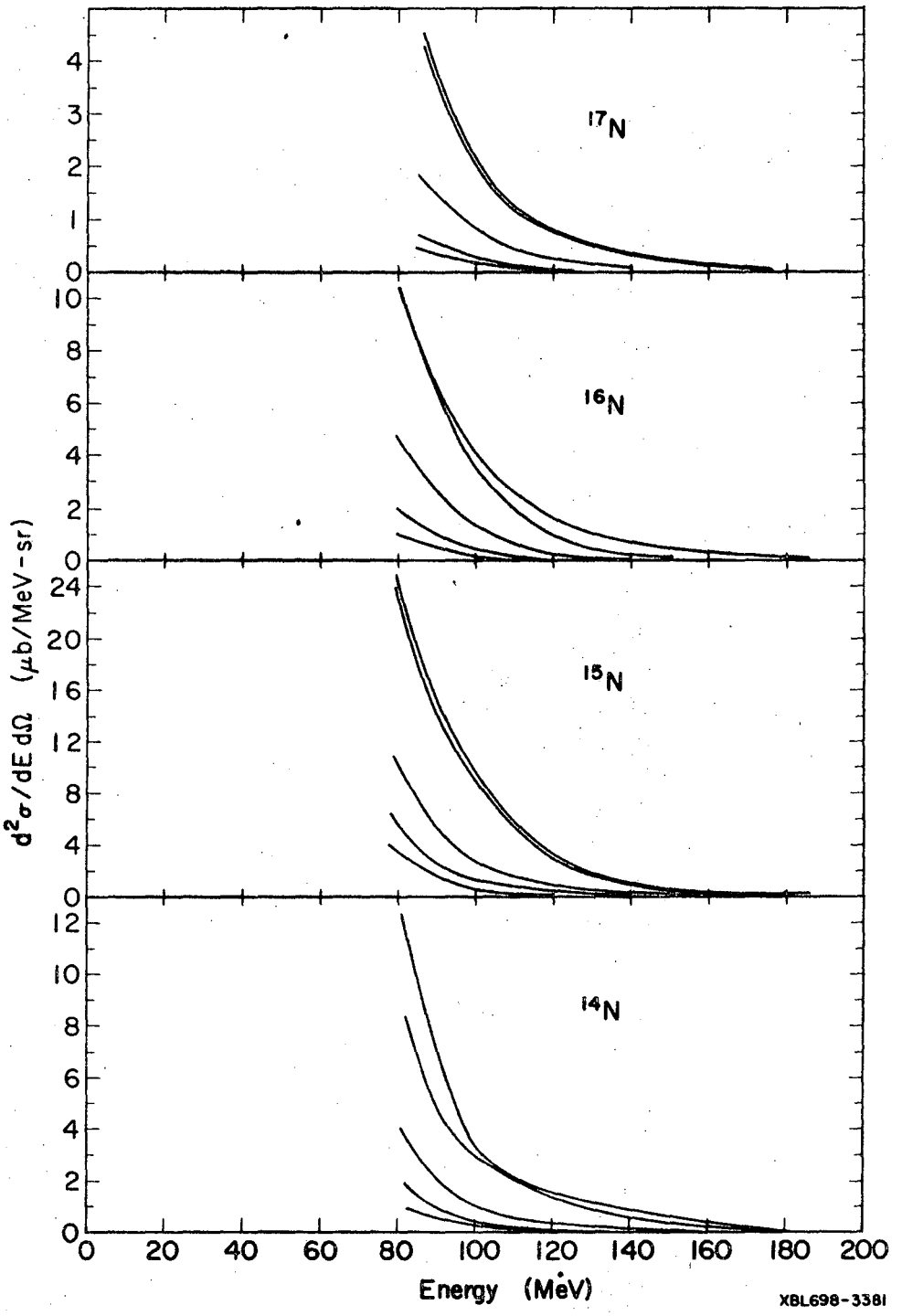
^{17}N
^{16}N
^{15}N
^{14}N
$d^2\sigma/dE\,d\Omega$ (μb/MeV-sr)
Energy (MeV)
XBL698-3381

Fig. 12

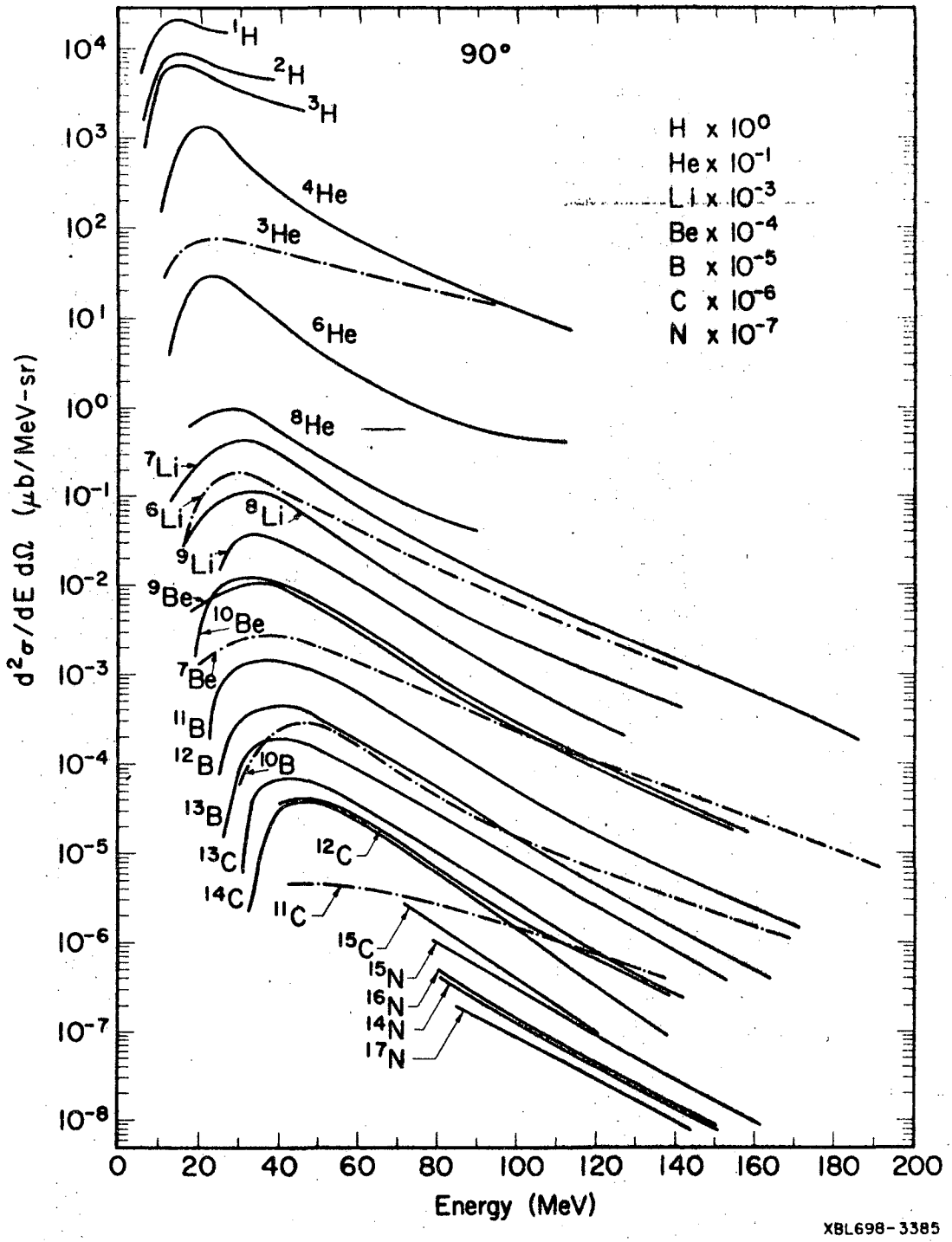
90°
H x 10^0
He x 10^-1
Li x 10^-3
Be x 10^-4
B x 10^-5
C x 10^-6
N x 10^-7
1H
2H
3H
4He
3He
6He
8He
7Li
6Li
8Li
9Li
9Be
10Be
7Be
11B
12B
10B
13B
13C
14C
12C
11C
15C
15N
16N
14N
17N
d²σ/dE dΩ (μb/MeV-sr)
Energy (MeV)
XBL698-3385

Fig. 13

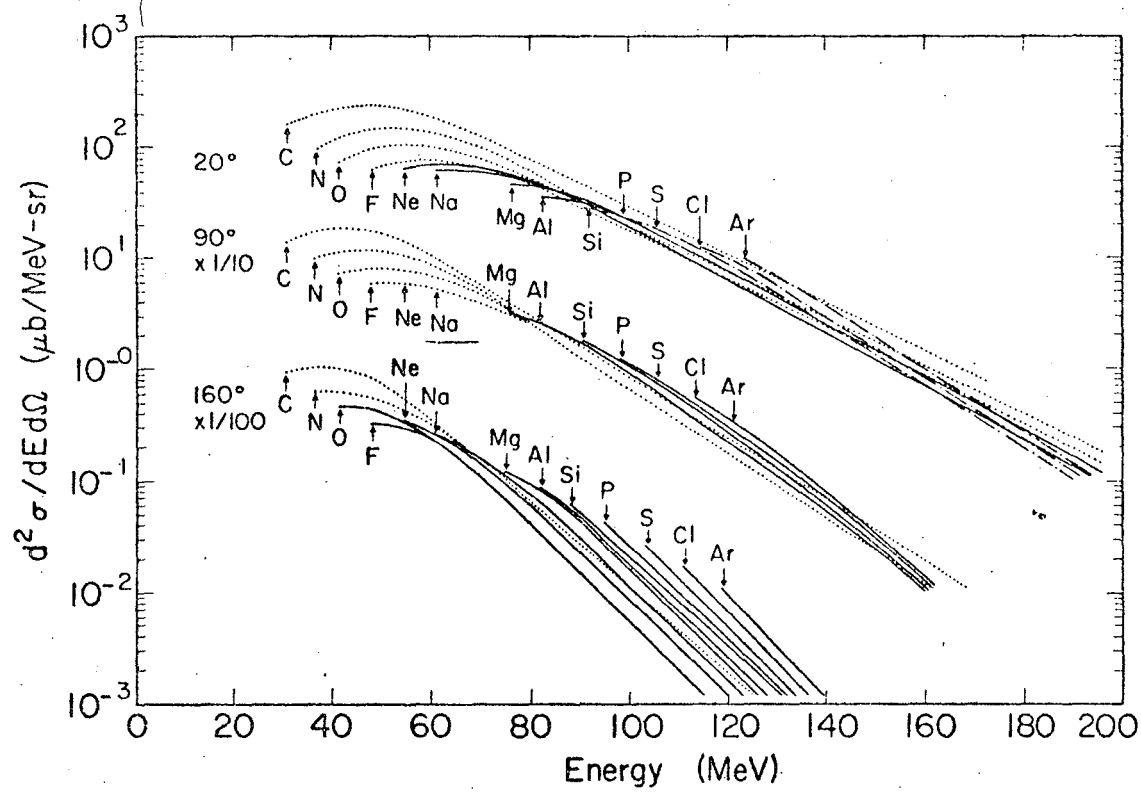

XBL698-3383

Fig. 14

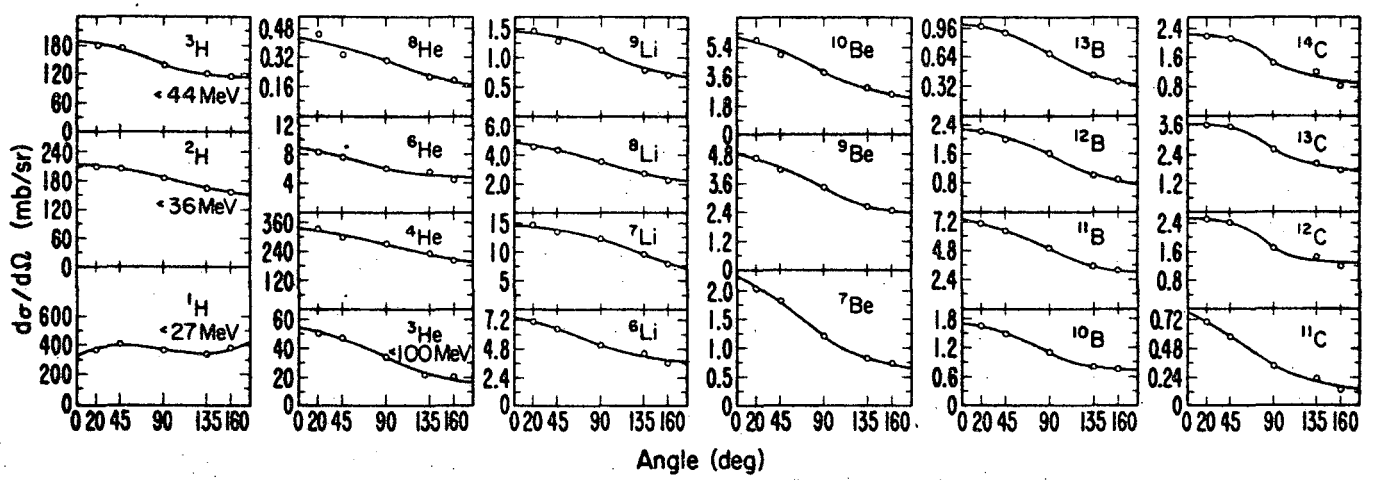

XBL 698-3434

Fig. 15

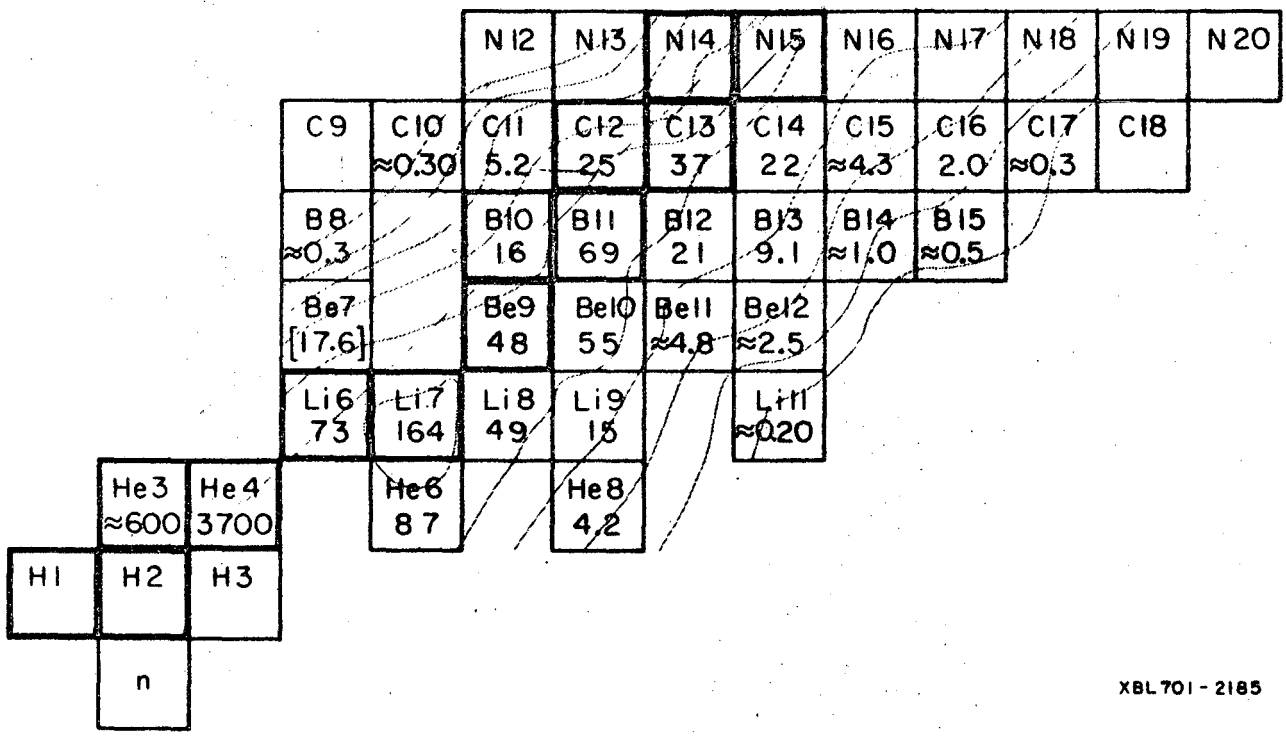
N12
N13
N14
N15
N16
N17
N18
N19
N20
C9
C10 ≈0.30
C11 5.2
C12 25
C13 37
C14 22
C15 ≈4.3
C16 2.0
C17 ≈0.3
C18
B8 ≈0.3
B10 16
B11 69
B12 21
B13 9.1
B14 ≈1.0
B15 ≈0.5
Be7 [17.6]
Be9 48
Be10 55
Be11 ≈4.8
Be12 ≈2.5
Li6 73
Li7 164
Li8 49
Li9 15
Li11 ≈0.20
He3 ≈600
He4 3700
He6 87
He8 4.2
H1
H2
H3
n
XBL701-2185

Fig. 16

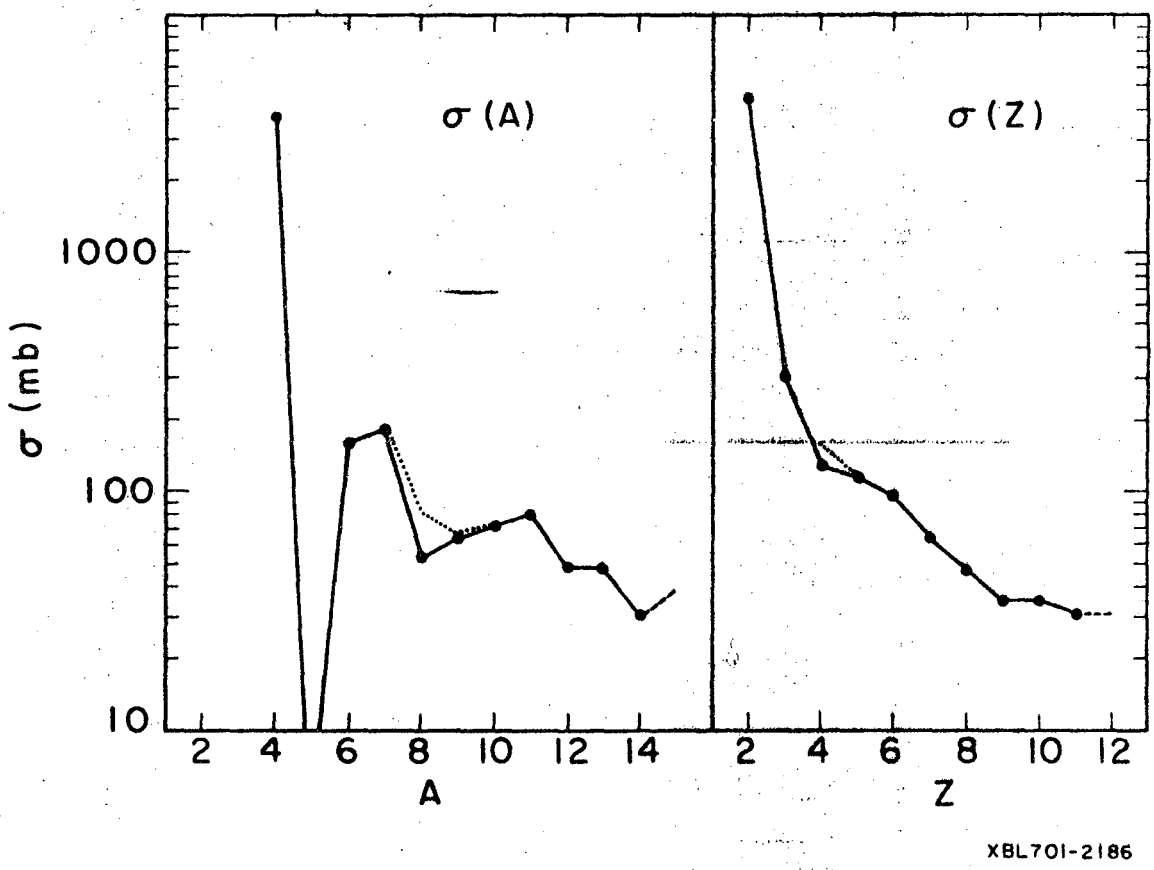

Fig. 17

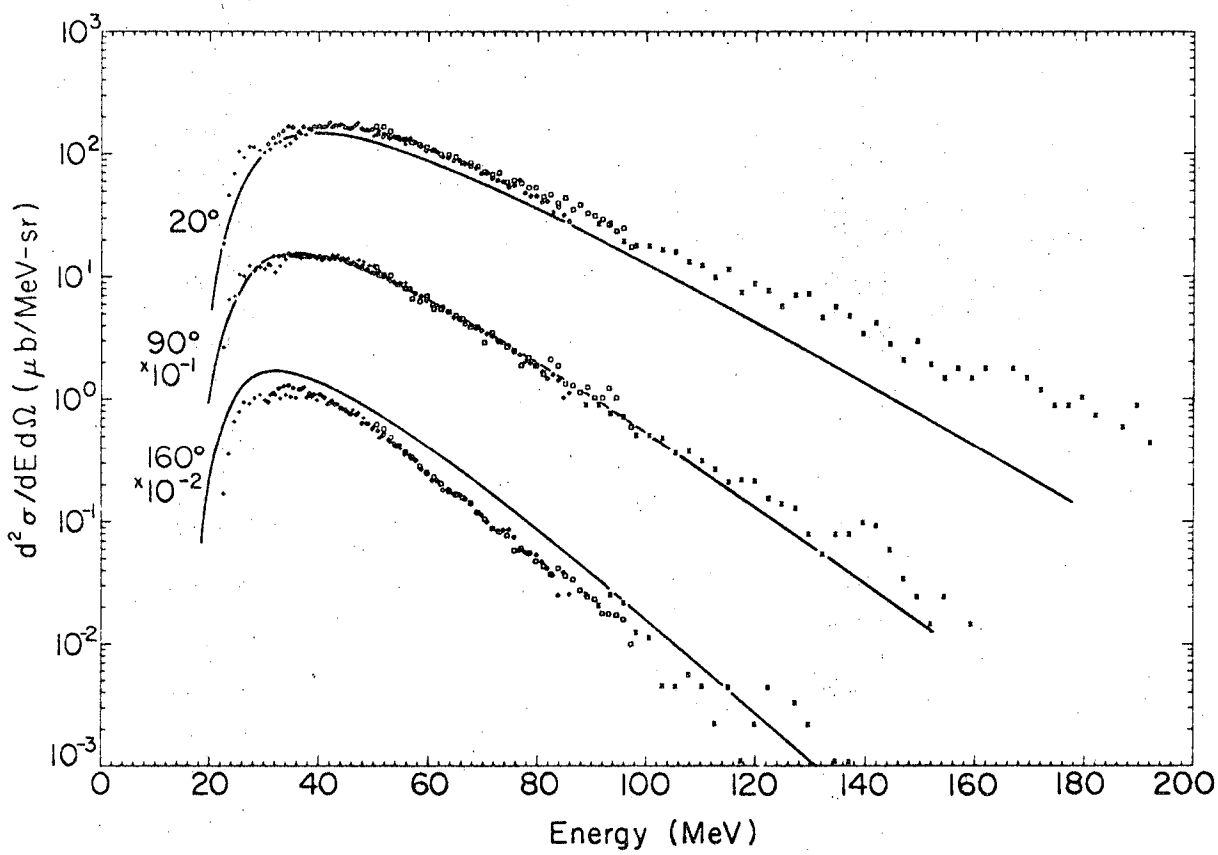

XBL705-2830

Fig. 18

LEGAL NOTICE

This report was prepared as an account of Government sponsored work. Neither the United States, nor the Commission, nor any person acting on behalf of the Commission:

A. Makes any warranty or representation, expressed or implied, with respect to the accuracy, completeness, or usefulness of the information contained in this report, or that the use of any information, apparatus, method, or process disclosed in this report may not infringe privately owned rights; or

B. Assumes any liabilities with respect to the use of, or for damages resulting from the use of any information, apparatus, method, or process disclosed in this report.

As used in the above, "person acting on behalf of the Commission" includes any employee or contractor of the Commission, or employee of such contractor, to the extent that such employee or contractor of the Commission, or employee of such contractor prepares, disseminates, or provides access to, any information pursuant to his employment or contract with the Commission, or his employment with such contractor.

TECHNICAL INFORMATION DIVISION
LAWRENCE RADIATION LABORATORY
UNIVERSITY OF CALIFORNIA
BERKELEY, CALIFORNIA 94720